The Pennsylvania State University

The Graduate School

John and Willie Leone Family Department of Energy and Mineral Engineering

NUMERICAL MODELING OF TIN-BASED ABSORBER DEVICES FOR COST-EFFECTIVE SOLAR PHOTOVOLTAICS

A Dissertation in

Energy and Geo-Environmental Engineering

by

Ramprasad Chandrasekharan

Submitted in Partial Fulfillment
of the Requirements
for the Degree of

Doctor of Philosophy

May 2012

The dissertation of Ramprasad Chandrasekharan was reviewed and approved* by the following:

Jeffrey R.S. Brownson
Assistant Professor of Energy and Mineral Engineering
Dissertation Advisor
Chair of Committee

Semih Eser
Professor of Energy and Geo-Environmental Engineering

Sarma Pisupati
Associate Professor of Energy and Mineral Engineering

Joan M. Redwing
Professor of Materials Science and Engineering

Yaw D. Yeboah
Professor and Department Head of Energy and Mineral Engineering

*Signatures are on file in the Graduate School

ABSTRACT

Due to the pressures of decreasing the electricity generation costs from solar photovoltaic (PV) modules, there is a need for novel light absorbing materials that can promise comparable conversion efficiencies at lower manufacturing costs than the incumbent technologies based on crystalline Si or thin films (CdTe or Cu-In-Ga-S). This research evaluates the tin-suite of absorber materials (based on tin monosulfide; SnS, and Cu-Zn-Sn-S; CZTS) as the next generation of PV cells that can yield the desired performance in the long term. Numerical models have been developed using Analysis of Microelectronic and Photonic Structures (AMPS-1D) to reveal efficiencies of cells under AM1.5 illumination based on three n-p heterojunctions: CdS|CdTe, CdS|SnS and ZnO|SnS, and identify avenues for further efficiency improvements in SnS PV. It has been predicted that PV devices based on the SnS (*absorber*)-ZnO (*oxide*) configuration yield higher conversion efficiencies (η=20.3%) compared to the inverted configuration *oxide-absorber,* with respect to the incidence of light. The difference has been attributed to variations in open-circuit voltages for the two situations, and suggests the adoption of the *absorber-oxide* design for further device development. The other approach to increasing open-circuit voltages in tin-based cells by using the wider band gap CZTS revealed upto 17.6% efficiency limits in FTO (F-doped SnO_2)-*oxide (ZnO)-sulfide(CdS)-absorber(CZTS)* baseline cells, lower than the *absorber-oxide* configuration in SnS-based PV. Modeling of the CZTS cells under inverted configuration showed remarkably poor efficiencies (~3%) due to high hole affinities in the absorber that promoted surface recombination at the absorber-metal ohmic contact. This observation suggests the requirement of smaller hole affinities and indicates optimal absorber band gaps of 1.2-1.3 eV for high-efficiency PV conversion. The optimal value should be achieved by cationic substitution of the tin sublattice with copper and/or zinc atoms rather than substituting sulfur with selenium in CZTS. It is concluded that future research efforts in device development should utilize the *absorber-oxide* design wherein the absorbers have the optimal band gaps as stated. The role of simulation tools such as AMPS will be crucial in aiding critical decision making on tin-based materials as solar PV continues to become an affordable source of electricity.

TABLE OF CONTENTS

LIST OF FIGURES

ACKNOWLEDGEMENTS

I would like to take this opportunity to thank a few people who have helped me through the course of my Ph.D. First and foremost, I express my sincere gratitude to my advisor Dr. Jeffrey Brownson for his invaluable guidance, support and encouragement that helped me achieve this goal. I would also like to thank my committee members, Dr. Semih Eser, Dr. Sarma Pisupati and Dr. Joan M. Redwing for agreeing to be a part of my dissertation committee and giving their valuable suggestions.

I am also thankful to the other members of the Brownson research group for their assistance during the course of my study. I am especially thankful to Mrs. Gretchen Macht for her cooperation and expertise in developing OPCAT models as part of our collaborative research on identifying the criticality of commodity materials used in thin film photovoltaics. I am eternally grateful to Dr. Stephen Fonash and his entire research group that developed the Analysis of Microelectronic and Photonic Structures – 1 Dimensional (AMPS-1D) simulation tool and made it available worldwide as a freeware for evaluating photovoltaic performance in optoelectronic device systems. My best wishes are certainly with the current group that is developing the three-dimensional version of the software.

The support extended by my family and friends deserves special mention. Their motivation and encouragement helped me remain competitive at all times and successfully complete this program.

Chapter 1

Introduction

Solar cells are photovoltaic (PV) devices that convert the electromagnetic radiation (i.e. light, including infrared, visible, and ultraviolet) from the sun into utilizable electrical energy. The conversion process can be considered as a sequence of the four basic steps:

1. ***light absorption*** that causes a transition from a ground state to an excited state in a material (the absorber of light),
2. the conversion of the excited state into at least one free electron-hole pair (***photogeneration***),
3. the presence of asymmetric forces in the device such that the produced free electrons travel in one direction and the produced free holes travel in the opposite direction (***separation***), and
4. completion of an external circuit by the combination of returning electrons with holes to return the absorber to the ground state (***non-equilibrium open system***).

1.1 The incident solar radiation

The energy supply from the sun is in the form of photons. The input is distributed over different wavelengths and depends on variables such as latitude, time of day, and atmospheric conditions. The accepted standards for common solar spectra have been developed by ASTM for the different amounts of radiation received at different altitudes on earth (defined by Air Mass; AM). ASTM Standard E490 is used for extra-terrestrial applications such as satellites and corresponds to AM0, while the standard terrestrial spectrum incident on the earth's surface is AM1.5G (global), based on standard ASTM G173 (cf. Figure 1.1).[1] The total radiation received on the earth's surface is an integral of the AM1.5G spectrum (sum of direct and diffuse components) and is called spectral power density, and equals 1000W/m^2 (peak Wattage; W_p). This value is used as the standard input radiation

incident on a solar cell (also referred to as irradiance), so that the performances of different devices can be fairly and conveniently compared, since the cells are now exposed to the same spectrum. The power output from a solar cell per unit area is usable electrical energy and is defined as the product of current density J and voltage V.

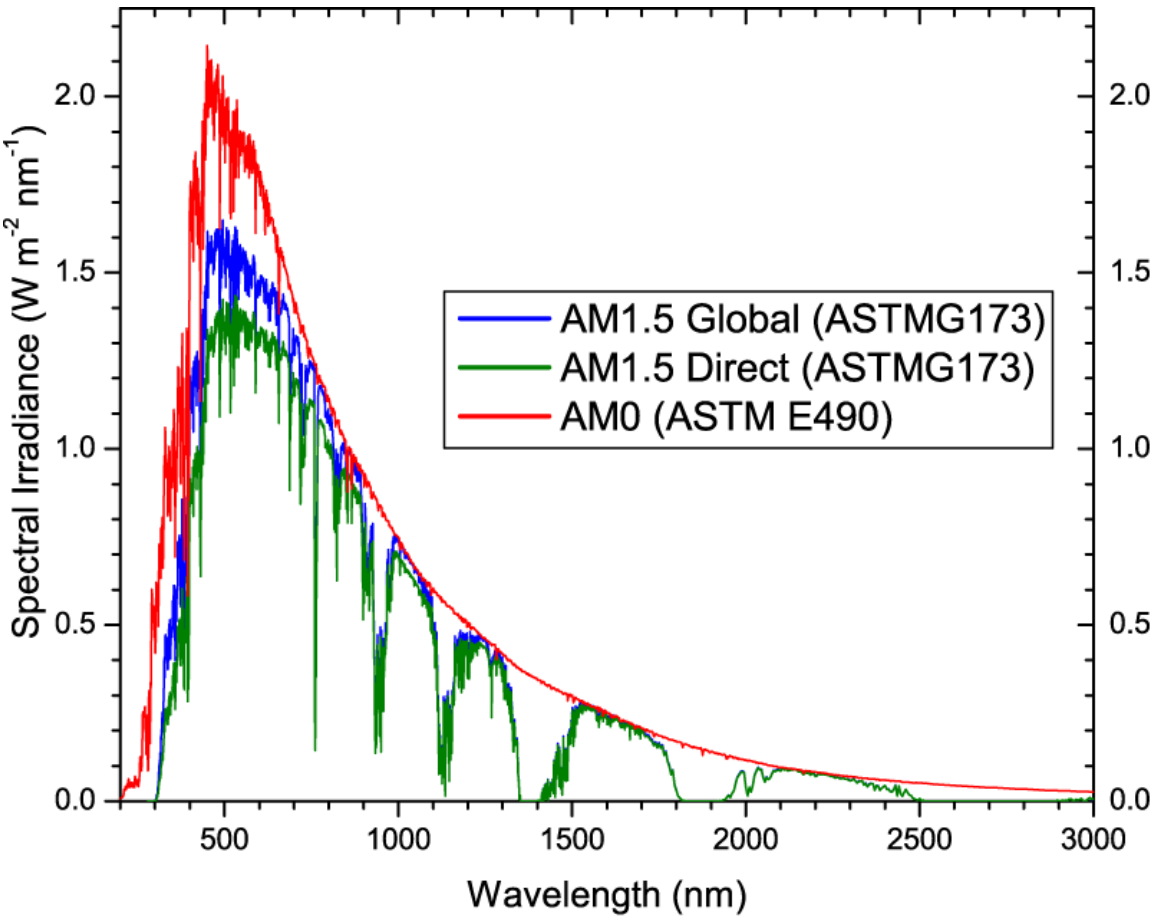

Figure 1.1: The standard terrestrial (AM1.5) and extraterrestrial (AM0) solar spectra.[2]

[Source: http://pvcdrom.pveducation.org/APPEND/Spectra.png, accessed Dec. 9, 2011]

1.2 The efficiency of a solar cell

Figure 1.2 shows a plot of the possible J-V operating points, called the "light" J-V characteristic of the PV cell. The points labeled J_{sc} and V_{oc} represent, respectively the extreme cases of no voltage produced between the opposite ends of the device (i.e. the illuminated cell is at short-circuit condition) and of no current flowing between the two ends (i.e. the illuminated cell is open-circuit condition).

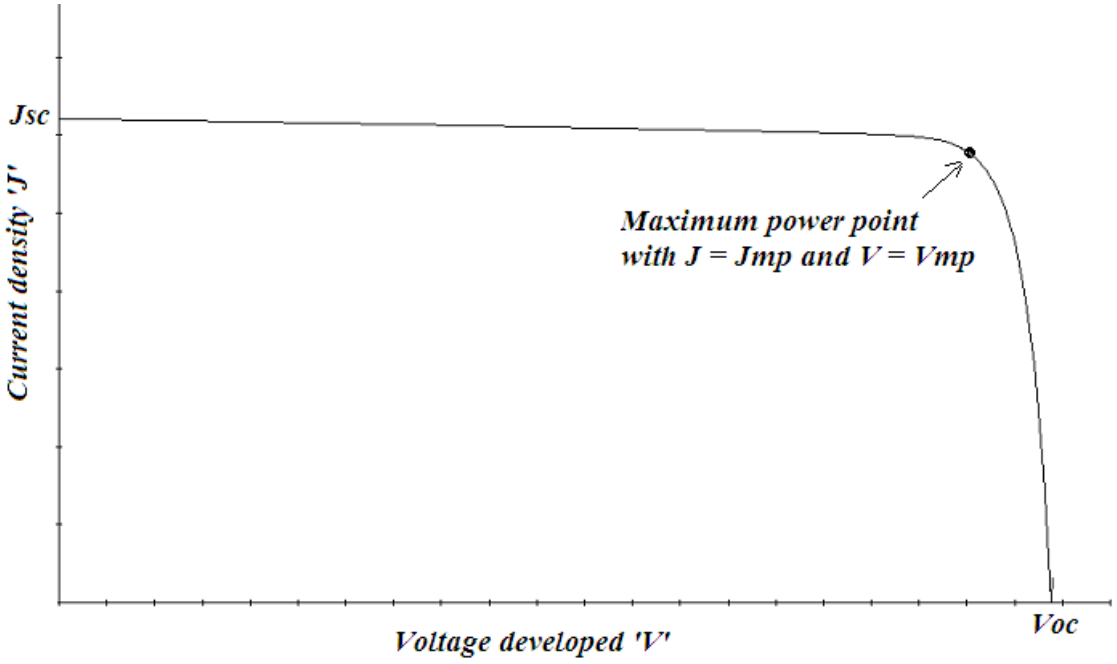

Figure 1.2: Typical J-V characteristic of a photovoltaic structure under illumination.

It must be noted that the power output (defined as J•V product at any point) has its highest value at the maximum power point corresponding to the values of J_{mp} and V_{mp} in Figure 1.2. The definition of these quantities helps define the thermodynamic efficiency η (eta) of the PV conversion process in terms of the input power P_{input} as:

$$\eta = J_{mp} \bullet V_{mp} / P_{input} \qquad \text{Eq. (1.1)}$$

It can be seen from Figure 1.2 that an ideal shaped J-V curve would be rectangular and would deliver a constant current density J_{sc} up to the open-circuit voltage V_{oc}. A term called the fill factor FF is hence used to measure how close a given characteristic is to conforming to this ideal rectangular J-V shape. The fill factor, by definition, is ≤ 1.

The efficiency of a PV device can now be defined in terms of the fill factor as:

$$\eta = FF \bullet J_{SC} \bullet V_{OC} / P_{input} \qquad \text{Eq. (1.2)}$$

It is evident that the two major parameters governing efficiencies in solar cells is the short-circuit current density J_{sc} and open-circuit voltage V_{oc}. Consequently, improvements to PV conversion efficiencies involve increasing J_{sc} or V_{oc} values, or both.

1.3 The different materials in a solar cell

1.3.1 Light absorber

The PV conversion process requires a number of materials having suitable electrical, electronic and optical properties that are fundamental to solar cell operation. The key material is the ***light absorber*** that is capable of excited states produced by photon absorption with energies in the photon-rich range of the solar spectrum (Figure 1.1). These excited states must be capable of being converted to free electrons and holes that can be collected externally. Commercial solar cells typically employ absorber materials that are inorganic semiconductors.

The ability of an absorber to absorb light of different wavelengths is defined by its absorption coefficient α that is a function of wavelength λ. Beer-Lambert's law is applied to calculate the absorbance A relative to the incident flux intensity I (photons impinging per cm^2 per second), some of which is reflected (R) off the material surface on which it is incident (always referred to as the "front'

end) and some transmitted (T) so that light emerges from the opposite side (always referred to as the "back" end) of the material.[1]

Based on this law, the absorbance A as a function of λ is given by:[1]

$$A(\lambda) = [I-R]\cdot[1-\exp(-\alpha(\lambda)d)] \qquad \text{Eq. (1.3)}$$

where d is the thickness of material traversed by the light radiation.

It is seen from eq. (1.3) that the absorption increases exponentially with α or material thickness d. It is therefore desirable to use thick material layers and/or semiconductors that have high absorption coefficients so that the value A can be maximized. The absorption length L_{abs} is a quantity used to denote absorption characteristics, and is defined as the thickness required to absorb 63% of the impinging light or equivalently required to develop 63% of the potential J_{sc} available.[1] This value corresponds to the α·d product equaling 1 in the exponent of eq. (1.3), so the absorption coefficient may be defined as the reciprocal of absorption length, and viceversa.

1.3.2 Schottky barrier

In addition to the absorber there are a number of other material components in a solar cell structure. They may include material layers that block one type of charge carrier while supporting transport of the other to help promote motion of one type of charge carriers in a different direction to the other. Such layers when used in conjunction with the absorber create a built-in electric field or chemical potential (an effective field) that breaks symmetry and forces electrons in one direction and holes in the other. This region is typically called a *junction* and forms the building block of a PV device system.[1]

1.3.3 Ohmic contacts

Conducting materials are typically used at either ends of the PV cell and provide the contacts of the cell electrodes and the grids needed for carrying the current to the external load. These materials must produce minimal electrical (voltage) and optical loss, and may be metals or transparent conductive oxides (TCOs). Metal are excellent ohmic contacts because of their low resistivity. It is a general rule that one must use a large work function metal as contact to p-type semiconductor materials (such as light absorbers).[1]

1.3.4 Transparent contacts

These materials are utilized to maximize light entry into the cell structure while still providing properly positioned electrodes.[1] They must have high transparencies, high conductivities and suitable work functions. Since absorption in these materials is achieved through doping (alloying), there is a trade-off between conductivity and light transmission. Some commonly employed materials for such roles include tin oxide, indium tin oxide (ITO) and fluorine-doped tin oxide (FTO).

A schematic of the different layers in a PV device is given in Appendix A, along with the nomenclatures and conventions used in this dissertation.

1.4 An overview of current commercial technologies

There are different solar cell technologies that have been developed based on different light absorbing materials and deployed commercially the world over. Over 80% of the global market is dominated by the first-generation panels that utilize crystalline silicon (c-Si) as the light absorbing constituent. Figure 1.3 shows a schematic of the most typical cell wherein the p-n junction is formed by doping the intrinsic silicon block (typically 180-200μm thick) with boron (to form the p-type layer) and phosphorous (to form the n-type layer), and joining the two layers together with their respective

contacts.[3] The silicon used in these cells may be monocrystalline or multicrystalline, with the former providing higher efficiencies due to their lower concentration of defects and other impurities that can increase the material's internal resistance.

However, the fastest growing PV technology is the second generation of solar cells that utilize thin films (2-5μm) of CdTe or Cu-In-Ga-S,Se (CIGS) as the light absorbing constituent. Figure 1.4 is a representation of the two devices that are typically built in the superstrate and substrate configurations, respectively. Note that the core junctions in the two stacks are the ones formed between the p-type absorber (CdTe or CIGS) and n-type "window" material (CdS) that is transparent to the light radiation (incident from the top in both cases). The TCO materials that also serve as ohmic contacts to electron transport are cadmium stannate in CdTe and ITO (In_2O_3-SnO_2 alloy) in CIGS. The hole contacts to the absorbers at the opposite end (to electron collection) of the two devices are copper and molybdenum.

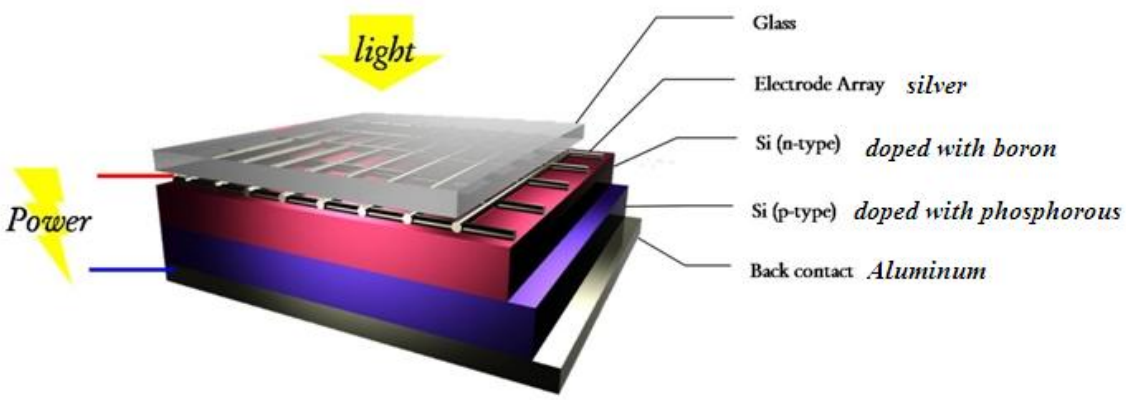

Figure 1.3: The typical crystalline Si solar cell based on p-n junction.[4]

[Source: http://www.shrinksolar.com/media/gen1-cell.jpg, accessed Dec. 9 2011]

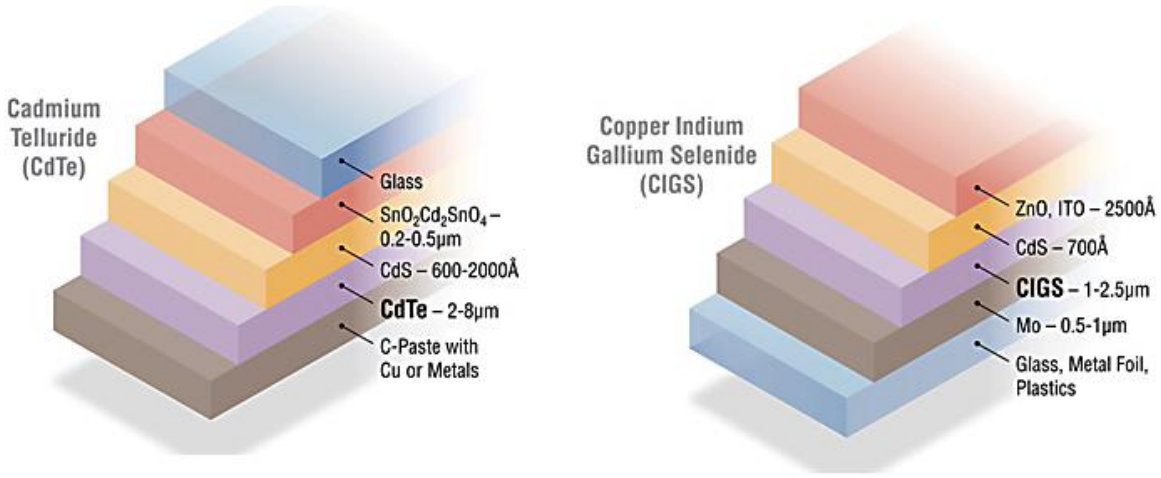

Figure 1.4: Schematic illustrations of typical CdTe (left) and CIGS (right) PV devices.[5]

[Source: http://www.nrel.gov/pv/thinfilm.html, accessed Dec. 9 2011]

The reasons for the much higher penetration rates of c-Si in the PV market are its much earlier maturation periods (1970s) compared to the thin films, which have been commercialized only in the past 5 years or so. The silicon cells typically also have higher efficiencies (25% [6]; mono-Si) compared to the record champion cell efficiencies for CdTe (17.3% [6]) or CIGS (20.3% [6]) devices. Current research efforts in the field of PV are heavily invested in improving the performance of the thin film technologies so that solar electricity can increasingly be an environmentally cleaner and more sustainable energy option.

1.5 The $/W$_p$ metric

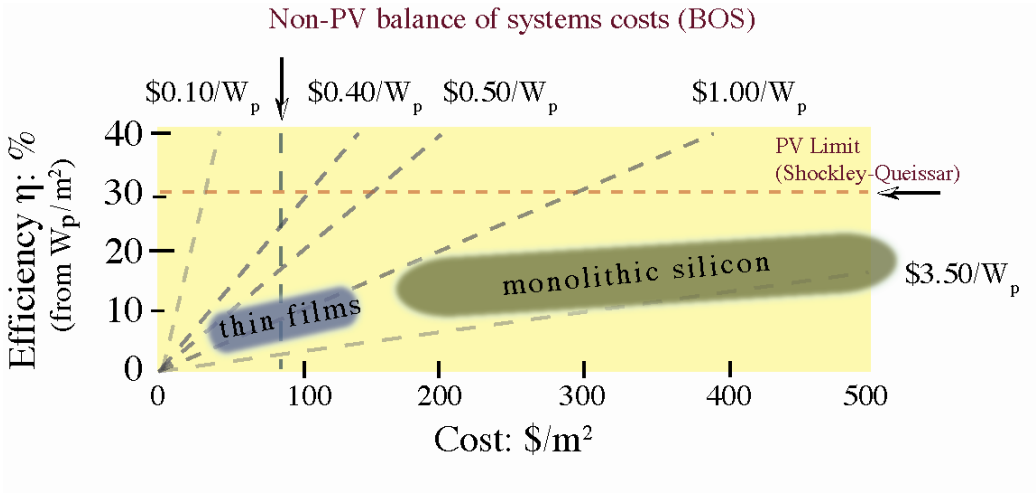

Figure 1.5: A comparison of efficiencies and production costs for the two generations of PV technologies.

The fundamental metric that determines the deployment of a particular technology is its cost of production per unit power produced from the solar cell. This parameter, $/W$_p$, normalizes the costs with respect to efficiency, and explains why thin film PV developed despite the maturing of the c-Si cells as an efficient technology. The higher efficiencies in c-Si are offset by the greater amounts of absorber used (two orders higher) relative to the thin films. Figure 1.5 shows a relative comparison of the metric (reciprocal of slope) for the two technologies. The 2011 cost-per-Watt as completely installed systems for the different technologies are $4.5/W$_p$ (mono-Si [7]), $3.38/W$_p$ (multi-Si [7]), and $3.30/W$_p$ (CdTe [7]).

It is interesting to note that even though CIGS is the fastest maturing technology and greater efficiencies have been achieved in this device compared to CdTe, it is still in the very early stages of commercialization due to the difficulties associated with vacuum-based deposition of the quaternary absorber layer over large areas, and the high costs and limited availability of indium relative to the demand levels of the industry.[8] It must also be considered that there is a typical 4-5% reduction in

efficiencies between the modules and the record efficiency cells for each technology.[3,6] This difference is due to a combination of losses in power while converting from direct current (DC) output of the cell to alternating current (AC) required for the electricity supply and wiring leakages, and highlights the difficulties in translating individual cell efficiencies onto large-area modules.

Further breakdown of the total installed costs in terms of just the module manufacturing costs indicates that it requires \$0.75 to produce $1W_p$ of power from CdTe cells (corresponding to module efficiencies of 12% and production costs of $\$90/m^2$ [9]), while multi-Si costs are at about $\$1/W_p$, as per 2011 prices. With the PV industry continuously experiencing downward cost pressure to remain competitive in the electricity markets, there is a need to reduce installed system costs below the \$0.4/Wp value (corresponding to full-system installed costs of $\$1/W_p$) for solar PV to be a sustainable option globally over the next decade and beyond.[9] There are two approaches to halving this value, either by (i) increasing the efficiencies, and/or (ii) decreasing the production cost.

An inspection of First Solar's Corporate Overview indicates cost-reductions from better material utilizations and increased production efficiencies of only 6-8% over the next 5 years.[9] This implies that greater improvements in PV conversion efficiencies have to be achieved to reduce $\$/W_p$ to the desired levels over the next several years. Considering the rate at which current module efficiencies are increasing (Figure 1.6) and the 3-4%-point lag with the champion cell values, it should be anticipated that cell efficiencies must cross the 20% barrier so that module efficiencies at ~15-16% can help improve the cost-effectiveness of PV electricity.

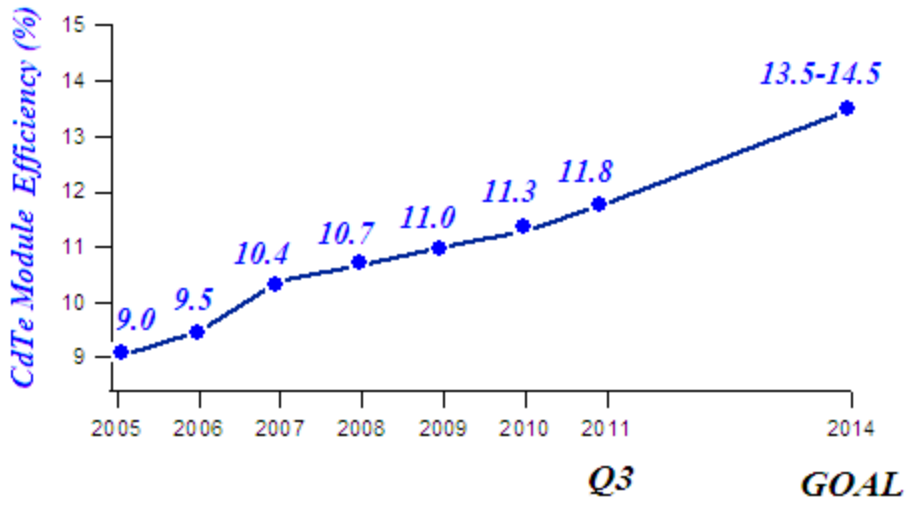

Figure 1.6: Recent trends in CdTe module efficiency improvements. [9]

This following work in Chapter 2 identifies the limitations in achieving the $\$/W_p$ goals with the incumbent technologies based on crystalline silicon and thin films (especially CdTe), and explains the need for alternative light-absorbing materials and the suitability of the tin-system as effective lower cost substitutes in the long run (>8 years). Chapter 3 provides a description of the simulation tool used in this research and the salient features of the software compared to other similar programs. Chapter 4 compares the numerical models developed for the CdTe and SnS-based systems, and proposes two-steps of improvements in the SnS PV devices to enhance conversion efficiencies. Above 20% PV conversion has been observed and explained in the SnS-ZnO devices modeled in Chapter 5, while Chapter 6 looks at the quaternary Cu-Sn-Zn-S absorber system and evaluates maximum efficiencies permitted by such devices. Chapter 7 highlights the major conclusions from this research and presents a path forward for tin-based PV research that can yield devices which can provide electricity at rates significantly lower than what is possible today.

References

[1] SJ Fonash. Solar Cell Device Physics. 2nd edition Elsevier, USA; **2010**.

[2] PVCDROM http://pvcdrom.pveducation.org/APPEND/Spectra.png (Accessed Dec. 9th **2011**)

[3] S Sandeep "*General Structure of Solar Cells"* March 2011. (Accessed Dec. 9th **2011**).

http://www.ncpre.iitb.ac.in/page.php?pageid=54&pgtitle=Si-Solar-Cells

[4] www.shrinksolar.com (Accessed Dec. 9th **2011**).

[5] www.nrel.gov (Accessed Dec. 9th **2011**).

[6] NREL: Best Research Cell Efficiencies. http://www.nrel.gov/ncpv/images/efficiency_chart.jpg. (Accessed Dec. 9th **2011**).

[7] B Prior. "*Cost and LCOE by Generation Technology*". 2009-2020 © GTM Research **2010**.

[8] USGS http://minerals.usgs.gov/minerals/pubs/commodity/indium/mcs-2011-indiu.pdf (Accessed Dec. 9th **2011**)

[9] First Solar Corporate Overview Q3 2011.

http://files.shareholder.com/downloads/FSLR/1522835684x0x477649/205c17cb-c816-4045-949f-700e7c1a109f/FSLR_CorpOverview.pdf (Accessed Dec. 10th **2011**).

Chapter 2

The need for alternative light absorbers and the suitability of tin-based material systems

The previous Chapter dealt with the long term economic goals of photovoltaic (PV) manufacturing and the projected increases in module efficiencies in the CdTe-based device systems. The need to decrease module prices to $\$0.4/W_p$, as explained in the previous Chapter, would require module efficiencies at 16-17% at production costs of $\$60\text{-}65/m^2$. Such module efficiencies would require 20% efficient cells at similar costs, considering the efficiency gap between modules and cells. However, the projected module efficiencies in CdTe are only 13.5-14.5% and constrained by the relatively low "champion cell" efficiencies of CdTe (17.3%). The scope for cost reductions in CdTe and CIGS-based systems is also severely restricted by the limited availabilities and rapidly increasing costs of refined tellurium and indium. Though there are no similar constraints in raw polysilicon availability, PV cells based on this material are close to their maximum efficiency limit, as will be explained in this Chapter. This Chapter evaluates the limitations to efficiency improvements and supply chain constraints in the crystalline silicon and thin film systems with respect to the projected cost reductions required of the PV industry over the next decade. This Chapter also explains the need for alternative light absorbing materials that can promise the required module efficiencies but can also be relatively cheaper and composed of earth-abundant and non-critical elements so that their deployment can make solar PV cost-effective and economically sustainable over the next several years.

2.1 Silicon solar cells: crystalline and amorphous (c-Si and a-Si)

The Si-based p-n homojunction PV cells have been long employed globally for producing electricity from solar energy. It is the most well-understood semiconductor technology in the world, benefitting

from decades of development by the integrated circuit (IC) industry. The advantages of Si-based PV include the availability of well-established techniques for controlling and manipulating the electronic and physical properties of doped homojunctions and the crustal abundance of the element on the earth's surface. Multicrystalline silicon (mc-Si) remains the global leader of PV products with a 45% market share that has reduced in the past few years with the rapid growth of the industry based on commercialization of the monocrystalline variety and the CdTe thin films.[1,2] The single crystal Si devices (sc-Si) have become increasingly popular because of their higher cell (and module) efficiencies (25 and 21% respectively) compared to mc-Si (20.5% and 17% respectively),[1] a trend that can be attributed to a combination of superior properties such as low internal resistance from defects and impurities and improvements in wire cutting technology that has enabled reductions in wafer thicknesses to about 180 µm at present.[1] It must be noted that ideal c-Si cells would require only about 20 µm of absorber material to absorb 95% of the incident radiation, based on their 'α' values that are typically 10^3 cm^{-1}. However, there is a thermodynamic limit on the maximum efficiency attainable with such single-junction cells, as explained by Shockley and Queisser (S-Q), in their 1961 paper.[3]

2.1.1 The S-Q limit

Figure 2.1 shows the maximum attainable efficiencies in Si and CdTe PV cells as a function of their optical band gaps (1.2 and 1.5 eV respectively). It can be seen that the limit is ~33% for Si and 31% for CdTe.

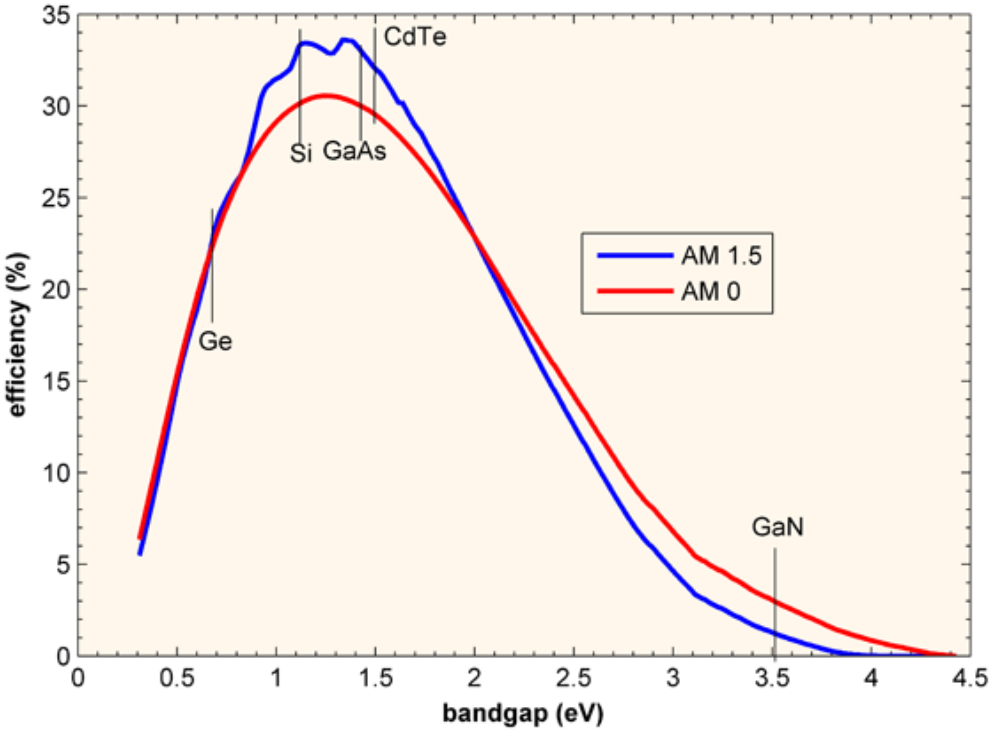

Figure 2.1: Thermodynamic efficiency limits (as calculated by S-Q) for single-junction solar cells as a function of band gap for AM1.5 (terrestrial) and AM0 (extraterrestrial) spectra.[4]

[Source: http://pvcdrom.pveducation.org/CELLOPER/Images/max_efficiency.png (Accessed Dec. 9 2011)]

Such a limit can be traced to Figure 1.2 in Chapter 1 where we notice a single point on the J-V characteristic at which the power output from the solar cell is maximum. This phenomenon is due to the fact that J and V have opposing trends as a function of absorber band gap; there is hence a need to select a semiconducting material having an optimal band gap that can maximize the power term. This optimal range is found to lie between 1.2 and 1.5 eV for terrestrial applications (Figure 2.1). If a semiconductor such as germanium (Ge; band gap 0.7 eV; shown in Figure 2.1) were selected for PV conversion, it would absorb most of the incident photons by virtue of its small band gap and generate free electron-free hole pairs. But, such charge carriers are in their excited states and need to be

separated and collected at their respective contacts before they can relax to their ground state, in a process referred to as ‘recombination’, at the end of their lifetimes (typically of the order of 100 ns -1 μs). This recombination process is a direct function of photogenerated carrier concentrations per unit volume of the material, and therefore smaller band gaps would imply greater recombination rates owing to increased carrier densities that causes the JV product to drastically reduce below the optimal limit. Conversely, the use of a wide gap semiconductor (such as GaN; shown in Figure 2.1) produces too few photogenerated charge carriers which causes current densities to be below the optimal values and thereby result in low conversion efficiencies. It is therefore evident that there is an optimal band energy gap in which the power output from a solar cell can be maximized relative to the irradiance, and this idea is visually depicted in Figure 2.2. Note that the plots in this figure are identical to the corresponding plots in Figure 1.1. Also, there is a direct relationship between the energy levels (x-axis) of Figure 2.1 and the wavelengths (x-axis) in Figure 2.2 and is given by:

$$E(eV) = 1239.8/\lambda(nm) \qquad \text{Eq. (2.1)}$$

where E is the energy of photons of the incident light radiation, in eV, and λ is the wavelength of light.

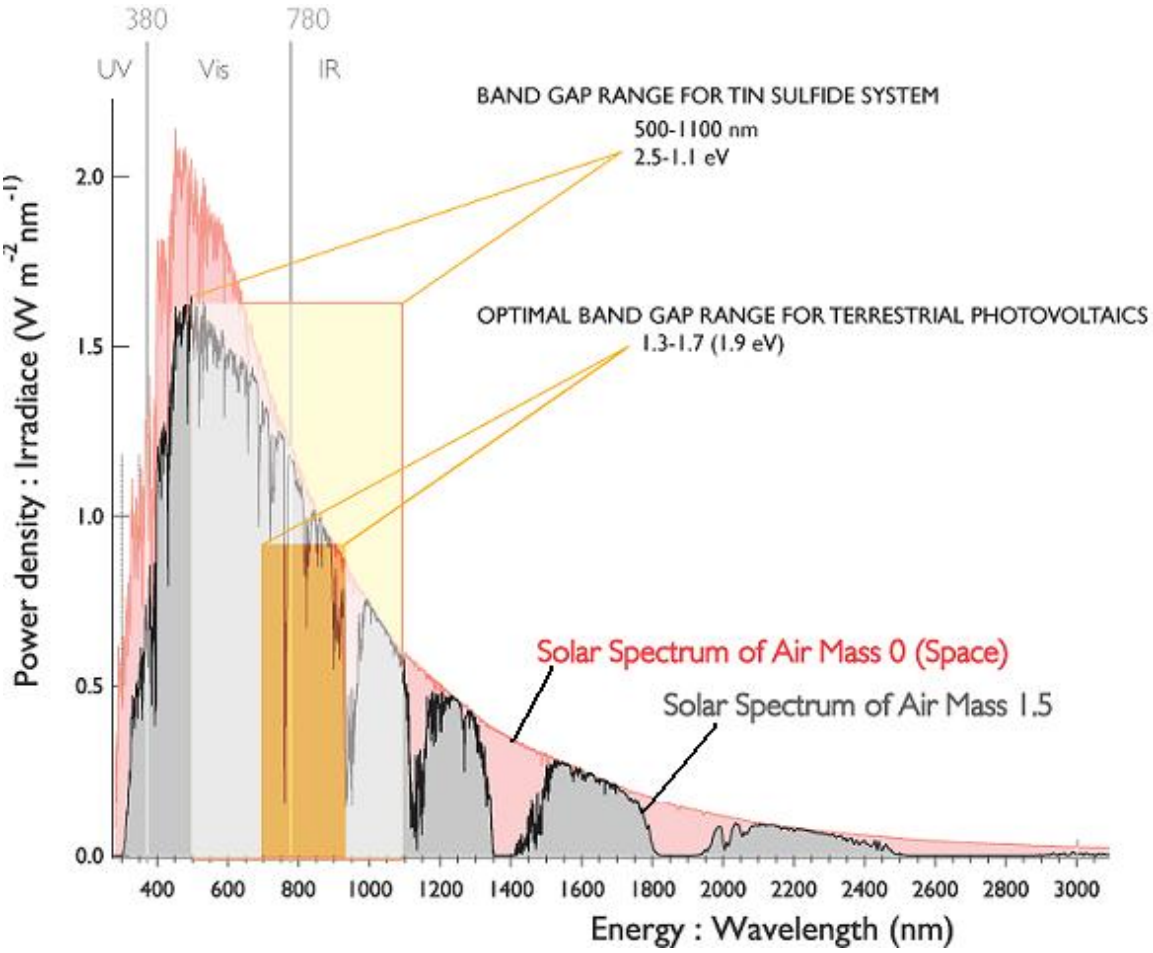

Figure 2.2: Terrestrial AM1.5 and extraterrestrial AM0 solar spectra with the band gap ranges of the different material systems.

It can now be concluded that the champion cells based on crystalline Si (η=25%) are close to 90% of their maximum efficiency values (η_{max}=33%), indicating little scope for efficiency improvements in such devices in future. However, the silicon cells utilize much greater quantities of the absorber (160-180 µm) than what is ideally required (20 µm), which suggests a lot of scope for material reductions. This difference is due to the inherent capability of the sawing process that can only produce wafers of such thicknesses and is associated with 50% material losses in the form of kerf. There is therefore a great requirement for the raw polysilicon feedstock that is used in the processing of refined silicon. The refining industry had been traditionally catering to the requirements of the IC market where

higher purity levels are desired and the recent transition (~2006-2007) from IC to solar PV as the major consumers of processed silicon caused short-term shortages and price spikes that severely strained the economic viability of silicon PV.[1] There are still efforts being pursued by silicon refiners to optimize their production techniques to the requirements of the solar industry, and it is not yet fully certain if the costs associated with polysilicon refining can keep pace with the reductions required in PV manufacturing over the next few years.

Solar cells based on hydrogenated amorphous silicon (a-Si) have been researched and developed as the cheaper variant compared to the better performing c-Si devices. Though cells made of this material are much less efficient (10% [1]) compared to c-Si, they employ films as thick as those used in thin film PV due to the much higher absorption coefficient of a-Si compared to the crystalline semiconductor. However, these cells suffer from light-induced degradation that eventually causes efficiencies to drop to 6-7% and stabilize in this range,[1] thereby resulting in significantly lower output. These cells have been surpassed subsequently by the emergence of CdTe in the past five years and are nowadays deployed only in small levels in specialized market segments where c-Si or CdTe may not be the best economic choice.[1]

A novel device that has been attracting recent research interest is the 'heterojunction with intrinsic thin layer' (HIT) solar cell.[5] This cell employs layers of p-type a-Si deposited on n-type c-Si to form a p-n a/c HJ that is sandwiched between intrinsic and n-type a-Si layers to form a tandem structure that has produced >20% conversion efficiencies recently.[6] However, tandem structures are typically high-efficiency high-cost cells due to the presence of multiple layers and the energy-intensive nature of their processing. This technology can be considered promising, but further cost reductions are required before they can become competitive enough with the incumbent devices.

The $\$/W_p$ value for the commercial c-Si in 2011 is about 1.3-1.5 (module) and 3.5-4.5 (fully-installed systems), as noted in Chapter 1. Based on the challenges confronting the PV technology based on

these cells, it is not fully certain if this material can permit cost reductions at rates required of the industry over the next decade. There is hence a need for thin film PV devices that employ CdTe or Cu-In-Ga-Se,S (CIGS) as the light absorbing material and can promise lowering of $\$/W_p$ values in the next few years.

2.2 CdTe photovoltaics

Cadmium telluride (CdTe) is a native p-type II-VI semiconducting material having an optical band gap 1.5eV that is optimal for photoharvesting and electricity generation. This material has a relatively high absorption coefficient ($\alpha > 10^4 cm^{-1}$) in the visible region of the solar spectrum that ensures much less quantities of the absorber (2-5μm) are actually required per cell compared to crystalline silicon. The ability to vaporize homogenously and its wide thermodynamic zone of stability suggest that simple evaporation processes may be easily used for film deposition of stoichiometric CdTe over large area substrates.[1]

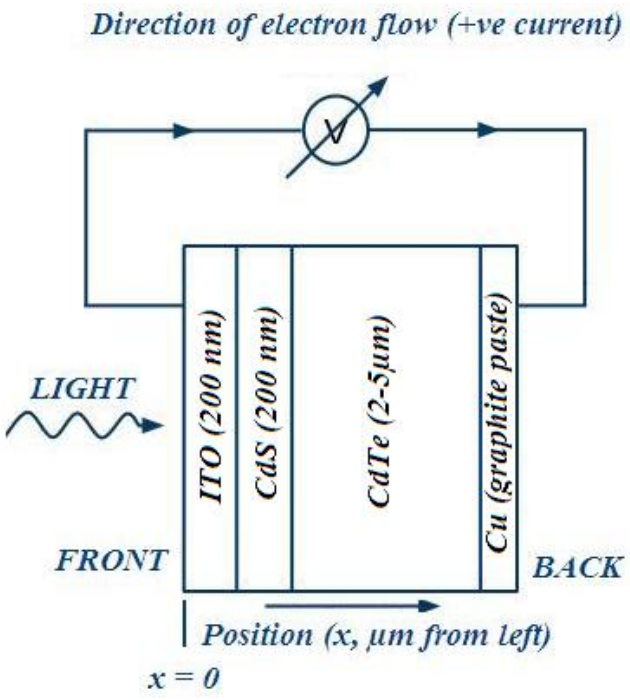

Figure 2.3: Typical structure of a CdTe solar cell.[7]

The standard CdTe-based device has the configuration shown in Figure 2.3. Cell production typically begins on a glass substrate on which a thin layer of 90:10 wt.% In_2O_3-SnO_2 (ITO) is usually sputtered as the transparent conductive oxide (TCO). The thickness of this layer is a tradeoff between conductivity and optical transmission. The n-type window layer CdS may then be deposited by a host of vacuum-based or wet chemical techniques such as physical vapor deposition (PVD), chemical bath deposition (CBD), close-space sublimation (CSS), sputtering, screen printing, or electrodeposition, though CSS at high temperatures (500-600^oC) is the most-widely used process for both CdS and CdTe thin films because of the high deposition rates (>20 μm/min) possible through convective vapor transport deposition.[1] The CdTe-CdS interface requires a $CdCl_2$ heat treatment step to increase absorber grain size and reduce defect density in the window layer. The final step in CdTe cell production is the formation of the low-resistance ohmic contact to carry the photogenerated current. Since CdTe has a high hole affinity (>5.4 eV, relative to local vacuum level), finding suitable metals for Ohmic contact formation is difficult as such a metal should have work function >5.4 eV. It is therefore necessary to produce a thin heavily doped p+-layer that is Te-rich on the surface of CdTe and typically involves one of wet chemical etching using bromine-methanol [7] or a mixture of nitric and phosphoric acids in water [8], or CBD of Te followed by post-deposition annealing [9]. This layer causes a back surface field across the region that aids hole transport from the absorber by serving as a tunneling barrier instead of the Schottky barrier. Different metals (Zn [10], Sb [11], Au [12], or most commonly Cu [12-14]) are then deposited from a graphite paste on this Te-rich layer to form a metal/metal telluride contact.

Thin film PV devices based on the CdS|CdTe heterojunction (HJ) have been researched for the past 30 years and record device efficiencies of 17.3% [15] have been recently produced. However, an inspection of the trend in record cell efficiencies reveals that CdTe research has virtually stagnated over the past 10 years (efficiency increase from 16.5% to 17.3%) due to the inability of the research community to increase the open-circuit (V_{OC}) values relative to absorber band gap (E_g).[16,17] This

"voltage deficit" (defined as $E_g/q - V_{oc}$, q: electronic charge) is 0.65V for CdTe cells, which is the highest when compared to c-Si or CIGS (0.45V) based devices [17]. This limitation can be attributed to the low free carrier density in CdTe (10^{14} cm^{-3}) that causes a space charge region upon HJ formation with CdS that is predominantly accommodated in the absorber. This phenomenon coupled with unfavorable band alignments at the rear contact can produce regions of high electric fields at either ends of the absorber that can cause high bulk recombination rates (further explained in Chapter 4). To avoid this undesirable feature, the absorber layer must be typically thicker (3-5 μm) than that observed in CIGS-based cells (1.5-2.5μm) so as not to compromise on the photovoltage and current density output. This restriction inhibits scope for manufacturing cost reductions in CdTe through lower material utilization. Together with the difficulties in achieving efficiency improvements beyond the 20% mark, it should be evident that achieving the two-fold cost-reduction in PV electricity from CdTe to ensure sustainable deployment should be highly unlikely, and highlights the need for CIGS or other novel light absorbing materials to drive the next wave of PV commercialization.

2.3 CIGS solar cells

$Cu(In_xGa_{1-x})(Se_xS_{1-x})$ or CIGS is a I-III-IV quaternary alloy compound formed by substituting gallium atoms in the indium sublattice of $CuInSe_2$ (CIS) that crystallizes in a stable chalcopyrite structure, and is In-rich at room temperature.[7] The purpose of the cation or anion substitution is to modify the band gap of CIS (1.02 eV) so that it lies in the optimal range for PV conversion. The electronic conductivity of these materials is explained in terms of their intrinsic defect chemistry. Copper and indium vacancies (i.e. excess selenium) yield strong p-type materials having carrier densities between 0.15 and $2x10^{17}$ cm^{-3}, while selenium vacancies produce n-type conductivity. The most important defect for carrier recombination is In_{Cu} (In at Cu antisite) due to both its low formation energy and its predicted level 0.34eV below the conduction band maximum (CBM), and results in a heavily compensated p-type material by passivation through the formation of $[2V_{Cu} + In_{Cu}]$ defect complexes.[18]

CIGS based photovoltaic devices are obtained by forming p-n heterojunctions with thin films of CdS, as shown Figure 2.4. As in CdTe devices the role of n-type CdS, which has a band gap of 2.4 eV, is not only to form the p-n junction with the absorber but also serve as a window layer that transmits incident light with relatively small absorption and reflection losses. Fabrication typically begins with the deposition of a Mo back contact followed by the p-type absorber, a thin window layer CdS (50-100 nm), with intrinsic or Al-doped ZnO serving as the transparent front contact. A conductive oxide layer of ITO may also be added to this contact to maximize absorption and in turn the current densities obtained from these cells. The advantage of CIGS lies in the flexibility of substrates (such as soda-lime glass, alumina foils, or high-temperature polyimide) on which these cells can be deposited.[1]

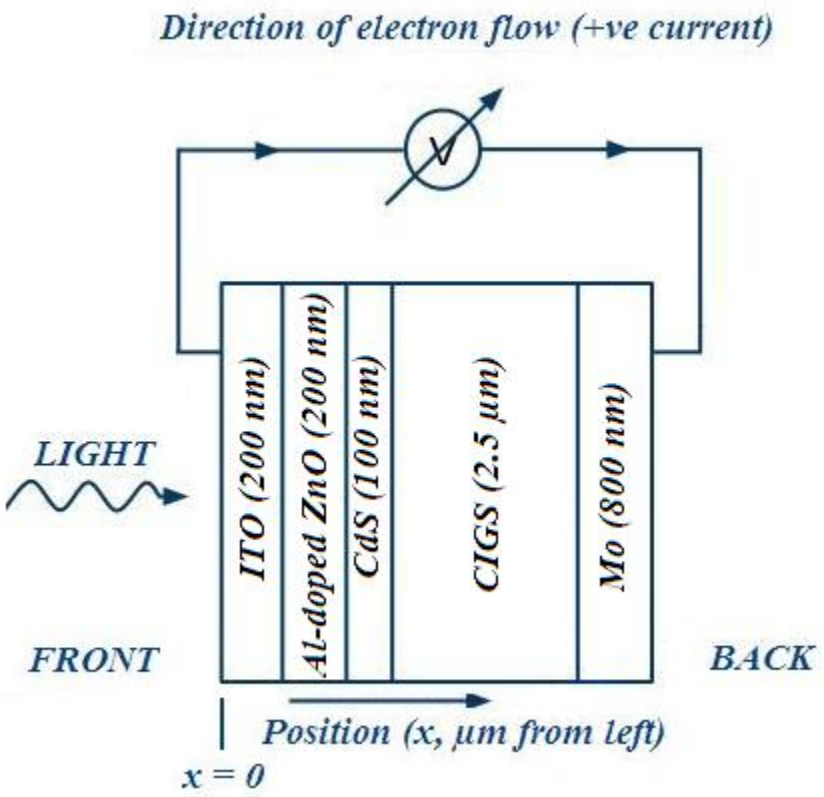

Figure 2.4: Typical structure of a Cu-In-Ga-S, Se (CIGS) cell.[7]

The best-efficiency CIGS cells employ absorber layers that have been deposited by the coevaporation process, [19] which typically consists of two stages. In the first step, the elemental fluxes are adjusted to be Cu-rich during the initial stage of the deposition at a substrate temperature of 350°C, forming a Cu-rich CIGS base film. In the final stage, the substrate temperature is raised to 450°C and the Cu:Ga/In flux ratio is reduced to less than 1 to produce large grains and stoichiometric films. The evaporation sources have cosine flux distributions whereby it is difficult to introduce sharp changes in composition or maintain uniformity over large areas under diffuse conditions of high vacuum.[1] Subsequent annealing for selenization (using Se or H_2Se vapors) requires excess amounts of the material. The excess demand is due to the low reactivity of Se with metals and leads to practical concerns such as material utilization. There are also toxicity concerns with using selenium; all the above factors have prevented cost-effective PV manufacturing based on CIGS.[1] Though solution-based approaches to deposition have been long adopted there are concerns with their scope for scaling up to commercial production levels (electrodeposition [20]) and the ability to produce dense, homogenous, and chemically graded structures.[1]

A comparison of the module (13.5% [1]) and champion cell efficiencies (20.3% [3]) indicates a 6-7% difference that can be attributed to the quality of the absorber layer. This difference in quality illustrates the challenges in translating the CIGS deposition process onto large-area substrates, and research efforts are focused on developing optimized and reproducible deposition processes that can permit large scale manufacturing. The energy and time-intensive nature of manufacturing such modules has prevented rapid commercialization of CIGS similar to what has been observed with the technologies based on CdTe and c-Si, despite CIGS yielding higher efficiency cells than the former.

2.4 Material availabilities for sustainable PV manufacturing

The global PV industry installed 18GW of grid-tied capacity in 2010,[21] with a major fraction of the installations employing the thin film-based panels constituting CdTe as the light absorbing material.

Such gigawatt levels of deployment are projected to be sustained and increase over the course of the next decade, suggesting greater demands on the raw material commodities cadmium and tellurium. Though higher quantities of silicon are used in PV manufacturing of c-Si cells compared to the thin film-based technologies, it is expected that there are no long term concerns with the availability of silicon and so this study only highlights the critical elements involved in the thin film cells.

2.4.1 Cadmium

Cadmium is a by-product of zinc ore mining and refining. It should be noted that at expected deployment levels over the next 5 years the annual demand for cadmium from the PV industry would still be small enough in proportion (<10%) to the overall global demand, which would suggest that the PV manufacturers might have to rely on demand (and price) levels being high enough so that production of the refined metal is economically feasible as part of the zinc smelting process.

2.4.2 Tellurium

Globally, all refined tellurium is a byproduct of copper ore processing. Despite copper being one of the more abundant metals in the earth's crust, tellurium is a highly scarce element due to its very low content in the copper ore concentrate (2 ppm). The estimated global production levels of refined tellurium are very low (about 1500 metric tonnes; MT annually), and present significant availability issues within the next 2-3 years as PV manufacturing expands its base worldwide. Further, 2011 prices of the refined metal are already high ($210,000/MT [22]), and constitute an increasing share of the PV manufacturing cost structure. With major supply bottlenecks expected soon due to a combination of increasing demand and dwindling tellurium reserves, it is highly likely that price escalations could render CdTe PV cost-prohibitive, and therefore even nullifying any improvements in manufacturing costs or device/module efficiencies.

2.4.3 Indium

There are similar concerns with indium availability and price levels and how they can increasingly erode the cost margins of the CIGS-based PV devices.[23] However, the ability to replace the metal with gallium in the absorber and their scope for increased recycling can slightly ease demand and availability concerns for CIGS PV. But, the material prices have been under constant pressure over the past 8 years due to increasing demand from the flat panel industry,[23] and any new demand such as for absorber layers could trigger a price explosion that can again remove the cost advantage of CIGS for PV deployment, similar to the situation with CdTe.

Given that the PV industry as a whole is experiencing record growth rates driven by environmental commitments and favorable incentives from governments over the past few years, there is an ever increasing downward pressure on manufacturing costs to ensure that growth rates can be sustained over the next decade and beyond. At the same time, there are also production and availability issues surrounding critical elements such as tellurium and indium that can trigger price explosions and render the PV technologies utilizing these materials unviable. This suggests that there is a growing need for alternative light absorbing materials that can yield devices of comparable (if not superior) efficiencies to the current thin film technologies at cheaper prices, and can be mass-manufactured from more earth-abundant and environmentally friendly materials. It is thus proposed in this dissertation that the tin-based absorber system could be an interesting choice to fill this gap, and that the material be investigated to identify PV conversion efficiencies relative to the incumbent cells.

2.5 Tin-based absorbers

2.5.1 Tin monosulfide

Preliminary investigation has shown that SnS offers abundant promise as a low cost light absorbing material for PV devices due to its robust band gap (~1.2 eV), scope for material processability, and

the higher availability and cheaper prices of the raw materials tin and sulfur. Tin monosulfide (SnS) is a native p-type II-VI semiconductor (like CdTe) having high absorption coefficients ($\alpha > 10^4$ cm^{-1}) in the visible and near-infrared bands (wavelengths 350–1100 nm), corresponding to the most intense region of the standard terrestrial solar spectrum that is incident on the earth's surface. The energy band structure of SnS (electron affinity χ = 4.2 eV and band gap E_g = 1.1-1.25 eV) makes it suitable for integration with n-type window materials having similar χ values and wider band gaps (>2.5 eV),[24] and can be tailored (to CZTS, as in CIGS) to lie in the 1.3-1.7 eV range for maximum efficiency. The reasonably high density of states (~10^{19} cm^{-3}) at the band edges and free hole carrier concentrations of 10^{16} cm^{-3} make SnS an effective photoconducting material for electron-hole pair generation and separation.[25] The inherent distortion in the structure due to weak interactions between the Sn (5s) and S (3p) orbital valence states makes the material amenable to band gap modifications by lattice dissolution from alloying.[25] Also, the 2010 commodity price of tin ($30/kg [26]) compares much more favorably with tellurium (>$200/kg [22]) and indium (~$700/kg [27]), and can be attributed to its much greater global reserve base and annual production in relation to the other two elements. A combination of such favorable optical and electronic properties and raw material prices makes tin sulfides an attractive proposition for the next generation of commercial thin film PV devices.

Owing to the higher free carrier concentrations (10^{16} cm^{-3}) in the absorber material, SnS permits thinner films (2 μm) relative to CdTe (5μm) for equivalent PV performance. Apart from the obvious advantage of lower commodity and processing costs of these SnS films, the use of thinner layers reduces bulk recombination rates in the absorber since the photogenerated charge carriers would now have to travel shorter distances to be separated at their respective contacts. The volatility of sulfur can be perceived as a significant processing issue especially when vapor-based techniques or post-deposition heat treatments are adopted, but chemically stable and stoichiometric CdS films have long been synthesized and studied and suggest that replicating the same with SnS should be practically

feasible. The higher carrier concentrations in SnS would also imply space charge regions of much smaller widths relative to that observed in CdTe, which means the tunneling probabilities for majority carrier injection from the absorber into the adjoining metal/p^+ layer is significantly enhanced and contributes to lower surface recombination rates and thereby higher voltages. It is therefore expected that the absorber-in-front configuration presents much less of a processing challenge and provides a great opportunity for improving voltages using SnS.

Research efforts on SnS to date have been scarce and fragmented and confined to developing synthesis protocols that enable deposition and characterization of micron thick monophase polycrystals on suitable substrates, so that they can be potentially developed for efficient PV performance. The techniques most commonly used for this purpose include electrochemical deposition,[28-38] chemical bath deposition (CBD),[39-42] thermal spray pyrolysis,[43-48] and plasma-enhanced chemical vapor deposition (PECVD).[49-51] The conductive nature and quality of films obtained, which determine the optical, electrical and electronic properties of the as-deposited SnS, were found to be dependent on the technique used and the experimental conditions employed. SnS films ranging from p-type conductivity and stoichiometries (Sn/S atomic ratio) lying between 1.0-1.4 to non-stoichiometric n-type films containing a mixture of phases (such as SnS_2, Sn_2S_3, Sn-oxysulfides) have been synthesized.[38,41,49] Monophase SnS films could be grown using PECVD at substrate temperatures beyond 200^{o}C, and usually exhibited near-stoichiometry (Sn/S atomic ratios < 1.1).[49] The near-stoichiometry is due to the fact that at lower temperatures (<200^{o}C) there is chlorine (Cl) incorporation (from the precursor $SnCl_4$) in the SnS, which is absent at higher temperatures because the Cl gets desorbed from the substrate surface due to the relatively high vapor pressures of $SnCl_x$ radicals.[49] However, for SnS deposition by thermal spray pyrolysis using liquid precursors, the best stoichiometric crystalline films were obtained in the temperature range 300-375^{o}C.[47] Films grown at lower temperatures were sulfur-rich due to the formation of secondary phases SnS_2 and Sn_2S_3, while those at higher temperatures suffered from sulfur deficiency due to the

co-formation of oxysulfide phases and sulfur re-evaporation, attributable to its high vapor pressure.[47] In fact, the high vapor pressure of sulfur is a major synthesis issue that restricts the range of processing temperatures that can be adopted for the formation of high quality monophase SnS films.

The majority of experimental work on SnS synthesis has therefore been based on solution-based techniques such as electrochemical and chemical bath depositions that permit growth of monophase crystalline films at much lower temperatures (<100^{o}C). However, only 500 nm thick SnS films have been grown by consecutive runs of CBD, suggesting the limited scope for scalability of this process. Also, the films deposited by this process suggest the presence of mixtures of the monosulfide with other sulfide phases.[42] ECD is therefore the most favored growth technique since it can be used to deposit micron thick films and allows good thermodynamic and kinetic control of the complex sulfur system, which is essential given the narrow thermodynamic zone of stability of SnS over a wide range of precursor compositions, pHs and temperatures. Though most experiments involving ECD are performed in the potentiostatic mode,[29-35,37] wherein a desired potential is applied and the current response monitored during deposition, uniform stoichiometric films have been obtained using the galvanostatic deposition mode because this technique allows kinetic control of the Sulfur-disproportionation reaction that is responsible for the formation of S^{2-} ions that ultimately react with Sn^{2+} in solution to form SnS upon application of current.[36]

A comparison of the optical absorption characteristics of the SnS films deposited using the various techniques reveals absorptivities uniformly greater than 10^5 cm^{-1} for incident photon energies higher than the band gap. Films grown by CBD and PECVD showed indirect transitions with band gaps of 1.12 eV and 1.16 eV respectively, while those grown by spray pyrolysis had direct band gaps between 1.3 and 2.0 eV depending on the substrate temperature and the relative fractions of the different phases in the as-deposited film. The use of ECD to deposit these sulfide films at much lower temperatures (50-90^{o}C) has yielded SnS having an indirect transition energy E_g~0.9-1.1 eV and a

direct band gap between 1.1 and 1.42 eV, depending on experiment temperature and pH. The acceptor carrier concentrations of these absorber layers arising due to the presence of native Sn^{2+} defects that are incorporated during deposition have typically been lower for thermally deposited films (6.3 x 10^{14}-1.2 x 10^{15} cm^{-3}) compared to the as-deposited films from ECD (7.3 x 10^{16} cm^{-3}),[24,25] a phenomenon attributable again to sulfur re-evaporation at higher temperatures. Since ECD permits excellent kinetic control of the aqueous sulfide system and yields the thickest stoichiometric films of SnS at near-ambient temperatures, the optical and electronic properties of the absorber used in this research correspond to the SnS films obtained using this technique.

With research in SnS confined to material synthesis and characterization, there is a need to first identify suitable materials that can be stacked with the absorber to form a PV device capable of producing electricity efficiently. Chapter 4 explains the modeling approach to evaluating conversion efficiencies in SnS-based junctions and identifies research pathways for improving efficiencies in this material system relative to the CdTe-based devices.

2.5.2 CZTS

Cu_2ZnSnS_4 (CZTS) is a promising semiconductor for low-cost and sustainable thin-film solar cell devices. All of the constituent elements of CZTS are naturally abundant and the band gap is close to the optimal single-junction value (~1.5 eV).[3] Replacing CZTS with selenium in the anion sublattice yields $Cu_2ZnSnSe_4$ (CZTSe), which adopts the same kesterite structure but has a smaller band gap (~1.0 eV).[52,53] Alloys of the two compounds, $Cu_2ZnSn(S,Se)_4$ (CZTSSe), have been attracting research attention and devices upto 9.6% efficiency have been obtained recently.[54]

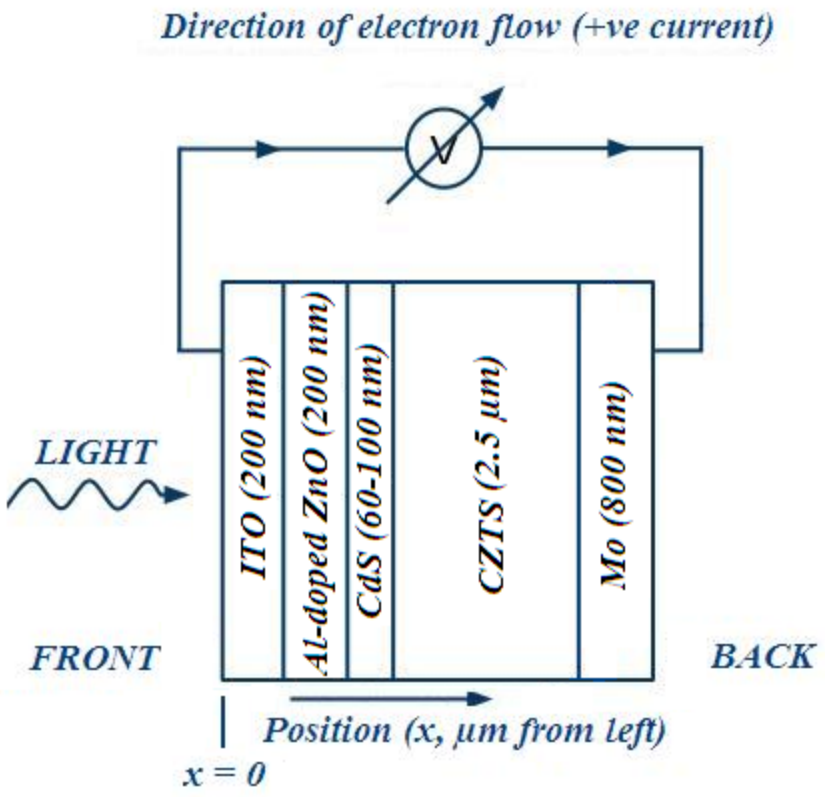

Figure 2.5: Schematic of the most efficient CZTS solar cell [54]

Figure 2.5 shows a schematic of the most efficient cells developed at IBM Research Labs.[54] It is interesting to note the similarity with CIGS cells (Figure 2.4) with respect to device configuration and materials used. The most common technique for depositing the quaternary layer is to co-RF sputter using SnS_2, Sn and ZnS targets in a N_2+H_2S atmosphere, [55] or co-evaporate the precursor metals in the nitrogen and sulfide atmosphere at temperatures between 330^{o}C and 550^{o}C because these techniques are considered scalable to large areas.[56] However, the most efficient cells illustrated above employ spin-coated absorbers synthesized from a slurry composed of Cu_2S-S and SnSe-Se solution mixtures in hydrazine.[54] The chemically reducing character of hydrazine stabilizes solutions of anions with direct metal-nonmetal bonding for select elements (e.g. Cu, Sn), without the necessity to introduce typical impurities such as Cl or O.[54] Low-temperature electrochemical routes to co-deposition of metals followed by annealing in S+N_2 atmosphere have also emerged in the last

couple of years.[57,58] However, many of these techniques suffer from significant stoichiometric deviations in the as-deposited films due to the presence of multiple sulfide phases of copper and/or zinc, and is attributed to the narrow thermodynamic zone of chemical stability of this material.[57,58]

A major focus of CZTS research is in understanding the defect chemistry responsible for the intrinsic conductivity observed in these compounds.[18,59-61] it has been thermodynamically calculated that the copper on zinc antisites (Cu_{Zn}) have significantly lower formation energy compared to copper vacancies (V_{Cu}) and Zn_{Sn}, predicting Cu_{Zn} as the most dominant defect type in these materials.[62] The kesterite differs from the chalcopyrite (CIGS) in this sense, as it is the copper vacancies that cause p-conductivity in the latter.[61] The different types of defects possible in CZTS and their transition levels within the band gap have been well established by Chen et al who suggest that electronic passivation of a number of these defects by defect-complex formation could render these layers as electrically benign as CIGS even under high non-stoichiometries and defect concentrations.[18] This property could be crucial to improving the efficiencies of CZTS cells through reduced recombinations in the absorber, and the ability to be stoichiometrically tolerant to charge transport could reduce the degree of thermodynamic and compositional control required during deposition and thereby facilitate process scale up for large areas.

It therefore appears that CZTS should be a highly promising candidate for the next-generation PV absorber because of its favorable properties for optical absorption and charge conduction. This material has attracted lot more research interest than the binary sulfide because of its wider band gap and the ability to compositionally tailor this value through selenium substitution. There is however little information on how CZTS performs as part of a thin film stack and the role of different material layers that contribute to PV conversion in such a device. This research looks at various CZTS device configurations for different contact materials in Chapter 5 with the objective of evaluating photoconversion efficiency limits in these structures and how this material compares with the binary sulfide as an effective absorber.

References

[1] CA Wolden, J Kurtin, JB Baxter, I Repins, SE Shaheen, JT Torvik, AA Rockett, VM Fthenakis, ES Aydil. "*Photovoltaic Manufacturing: Present status, future prospects, and research needs*". J. Vac. Sci. Technol. A 29 (3); 030801 (1-16); **2011.**

[2] B Prior. "*Cost and LCOE by Generation Technology*". 2009-2020 © GTM Research **2010.**

[3] W Shockley, HJ Queisser. "*Detailed Balance Limit of Efficiency of p-n Junction Solar Cells"*. J. Appl. Phys. 32 (3); 510-519; **1961.**

[4] PVCDROM http://pvcdrom.pveducation.org/CELLOPER/Images/max_efficiency.png (Accessed Dec. 9th **2011**).

[5] RW Miles, G Zoppi, I Forbes. "*Inorganic photovoltaic cells*". Mat. Today. 10 (11); 20-27; **2007**.

[6] Y Tsunomura, Y Yoshimine, M Taguchi, T Kinoshita, H Kanno, H Sakata, E Maruyama, M Tanaka. "22%-EFFICIENCY HIT SOLAR CELL". White Paper Sanyo. http://us.sanyo.com/Dynamic/customPages/docs/solarPower_22_3_Cell_Efficiency_White_Paper_Dec_07.pdf (Accessed Dec. 11th 2011)

[7] RW Birkmire, E Eser. "*Polycrystalline Thin Film Solar Cells: Present Status and Future Potential*". Annu. Rev. Mater. Sci. 27;625-53; **1997.**

[8] DL Bätzner, R Wendt, A Romeo, H Zogg, AN Tiwari. "*A study of the back contacts on CdTe/CdS solar cells*". Thin Solid Films. 361-362; 463-467; **2000**.

[9] R Ochoa-Landın, O Vigil-Galan, YV Vorobiev, R Ramırez-Bon. "*Chemically-deposited Te layers improving the parameters of back contacts for CdTe solar cells*". Sol. Energy 83; 134–138; **2009**.

[10] TA Gessert, P Sheldon, X Li, D Dunlavy, D Niles, R Sasala, S Albright, B Zadler. "*STUDIES OF ZnTe BACK CONTACTS TO CdS/CdTe SOLAR CELLS*". 26th IEEE PV Spec. Conf.; **1997.**

[11] N Romeo, A Bosio, V Canevari, A Podestà. "*Recent progress on CdTe/CdS thin film solar cells*". Sol. Energy 77; 795–801; **2004.**

[12] A Niemegeers, M Burgelman. "*Effects of the Au/CdTe Back Contact on IV and CV Characteristics of Au/CdTe/CdS/TCO Solar Cells*". J. Appl. Phys. 81 (6); 2881-2886; **1997.**

[13] SE Asher, FS Hasoon, TA Gessert, MR Young, P Sheldon, J Hiltner, J Sites. "*Determination of Cu in CdTe/CdS Devices Before and After Accelerated Stress Testing*". 28th IEEE PV Spec. Conference; 479–482; **2000**.

[14] TA Gessert, MJ Romero, RG Dhere, SE Asher. "*Analysis of the ZnTe: Cu Contact on CdS/CdTe Solar Cells*". NREL Tech. Rep. No. NREL/CP-520-33940; **2003.**

[15] HC Chou, A Rohatgi, NM Jokerst, EW Thomas, S Kamra. "*Copper Migration in CdTe Heterojunction Solar Cells*". J. Electr. Mater. 25(7); 1093–1098; **1996.**

[16] NREL: Best Research Cell Efficiencies. http://www.nrel.gov/ncpv/images/efficiency_chart.jpg (Accessed Dec. 9th **2011**)

[17] AL Fahrenbruch. "*Exploring Back Contact Technology to Increase CdS/CdTe Solar Cell Efficiency*" Proc. MRS; Y7-5; **2007.**

[18] I Repins, N Vora, C Beall, S-H Wei, Y Yan, M Romero, G Teeter, H Du, B To, M Young, M Noufi. "*Kesterites and Chalcopyrites: A Comparison of Close Cousins*". NREL Preprint, Presented at the Mat. Res. Soc. Spring Meeting **2011**.

[19] MA Contreras, B Egaas, K Ramanathan, J Hiltner, A Swartzlander, F Hasoon, R Noufi. "*Progress Toward 20% Efficiency in Cu(In,Ga) Se_2 Polycrystalline Thin-Film Solar Cells*". Prog. in PV 7; 311; **1999**.

[20] RN Bhattacharya. "*Solution Growth and Electrodeposited $CuInSe_2$Thin Films*". J. Electrochem. Soc. 130 (10); 2040-2042; **1983**.

[21] W Palz. "*PV Markets Worldwide: Where We Stand*". Solar Today 25 [7]; 20; **2011**.

[22] USGS http://minerals.usgs.gov/minerals/pubs/commodity/selenium/mcs-2011-tellu.pdf (Accessed Dec. 9th **2011**)

[23] MA Green. "*Estimates of Te and In Prices from Direct Mining of Known Ores*". Prog. In PV: Res. Appl.; 17; 347–359; **2009**.

[24] M Devika, KTR Reddy, NK Reddy, K Ramesh, R Ganesan, ESR Gopal, KR Gunasekhar. "*Microstructure Dependent Physical Properties of Evaporated Tin Sulfide Films*". J. Appl. Phys. 100; 023518 (1-7); **2006**.

[25] A Walsh, GW Watson "*Influence of the Anion on Lone Pair Formation in Sn (II) Monochalcogenides: A DFT Study*" J. Phys. Chem. 109; 18868-18875; **2005**.

[26] USGS http://minerals.usgs.gov/minerals/pubs/commodity/tin/mcs-2011-tin.pdf (Accessed Dec 9th **2011**).

[27] USGS http://minerals.usgs.gov/minerals/pubs/commodity/indium/mcs-2011-indiu.pdf (Accessed Dec. 9th **2011**).

[28] B Subramanian, C Sanjeeviraja, M Jayachandran "*Cathodic Electrodeposition and Analysis of SnS Films for Photoelectrochemical Cells*". Mat. Chem. & Phys. 71; 40–46; **2001.**

[29] A Ghazali, Z Zainal, MZ Hussein, A Kassim. "*Cathodic Electrodeposition of SnS in the Presence of EDTA in Aqueous Media*". Sol. Energy Mat. & Sol. Cells 55; 237-249; **1998.**

[30] M Ichimura, K Takeuchi, Y Ono, E Arai. "*Electrochemical Deposition of SnS Thin Films*". Thin Solid Films 361-362; 98-101; **2000**.

[31] K Takeuchi, M Ichimura, E Arai, Y Yamazaki "*SnS Thin Films Fabricated by Pulsed and Normal Electrochemical Deposition*" Sol. Energy Mat. & Solar Cells 75; 427–432; **2003.**

[32] N Sato, M Ichimura, E Arai, Y Yamazaki. "*Characterization of Electrical Properties and Photosensitivity of SnS Thin Films Prepared by the Electrochemical Deposition Method*". Sol. Energy Mat. & Sol. Cells 85; 153–165; **2005.**

[33] M Gunasekaran, M Ichimura. "*Photovoltaic Cells Based on Pulsed Electrochemically Deposited SnS and Photochemically Deposited CdS and* $Cd_{1-x}Zn_xS$". Sol. Energy Mat. & Sol. Cells 91; 774–778; **2007**.

[34] S Cheng, G Chen, Y Chen, C Huang. "*Effect of Deposition Potential and Bath Temperature on The Electrodeposition of SnS Film*". Opt. Mat. 29; 439–444; **2006.**

[35] S Cheng, Y He, G Chen, E-C Cho, G Conibeer. "*Influence of EDTA Concentration on The Structure and Properties of SnS Films Prepared by Electrodeposition*". Surf. & Coat. Technol. 202; 6070–6074; **2008**.

[36] JRS Brownson, C Georges, G Larramona, A Jacob, B Delatouche, CL-Clément. "*Chemistry of Tin Monosulfide (δ-SnS) Electrodeposition*". J. Electrochem. Soc. 155 (1); D40-D46; **2008.**

[37] S Cheng, Y He, G Chen. "*Structure and Properties of SnS Films Prepared by Electrodeposition in Presence of EDTA*". Mat. Chem. & Phys. 110;449–453; **2008.**

[38] JRS Brownson, C Georges, CL-Clément. "*Synthesis of a δ-SnS Polymorph by Electrodeposition*". Chem. Mater. 18; 6397-6402; **2006.**

[39] M Ristov, G Sinadinovski, M Mitreski, M Ristova. "*Photovoltaic Cells Based on Chemically Deposited p-type SnS*" Sol. Energy Mat. & Sol. Cells 69; 17-24; **2001.**

[40] A Tanusevski. "*Optical and Photoelectric Properties of SnS Thin Films Prepared by Chemical Bath Deposition*". Semicond. Sci. Technol. 18; 501–505; **2003.**

[41] MTS Nair, CL-Mata, O Daza, PK Nair. "*Copper Tin Sulfide Semiconductor Thin Films Produced by Heating SnS–CuS Layers Deposited From Chemical Bath*". Semicond. Sci. Technol. 18; 755–759; **2003.**

[42] D Avellaneda, G Delgado, MTS Nair, PK Nair. "*Structural and Chemical Transformations in SnS Thin Films Used in Chemically Deposited Photovoltaic Cells*". Thin Solid Films 515; 5771–5776; **2007.**

[43] S Lopez, A Ortiz. "*Spray Pyrolysis Deposition of Sn_xS_y Thin Films*". Semicond. Sci. Technol. 9; 2130-2133; **1994.**

[44] NK Reddy, KTR Reddy. "*Growth of Polycrystalline SnS Films by Spray Pyrolysis*" Thin Solid Films 325; 4–6; **1998.**

[45] B Thangaraju, P Kaliannan. "*Spray Pyrolytic Deposition and Characterization of SnS and SnS_2 Thin Films*". J. Phys. D: Appl. Phys. 33; 1054–1059; **2000.**

[46] KTR Reddy, PP Reddy, RW Miles, PK Datta. "*Investigations on SnS Films Deposited by Spray Pyrolysis*". Opt. Mat. 17; 295-298; **2001.**

[47] NK Reddy, KTR Reddy. "*SnS Films for Photovoltaic Applications: Physical Investigations on Sprayed SnxSy Films*". Physica B 368; 25-31; **2005.**

[48] KTR Reddy, NK Reddy, RW Miles. "*Photovoltaic properties of SnS based Solar Cells*". Sol. Energy Mat. & Sol. Cells 90; 3041–3046; **2006.**

[49] A Ortiz, JC Alonso, M Garcia, J Toriz. "*Tin Sulfide Films Deposited by Plasma-Enhanced Chemical Vapor Deposition*". Semicond. Sci. Technol. 11; 243-247; **1996.**

[50] AS-Juarez, A Ortiz "*Structural Properties of Sn_xS_y Thin Films Prepared by Plasma-Enhanced Chemical Vapor Deposition*". J. Electrochem. Soc. 147 (10); 3708-3717; **2000.**

[51] AS-Juarez, AT-Silver, A Ortiz. "*Fabrication of SnS_2/SnS Heterojunction Thin Film Diodes by Plasma-Enhanced Chemical Vapor Deposition*". Thin Solid Films 480-481; 452-456; **2005.**

[52] S Chen, XG Gong, A Walsh, and S-H Wei. "*Crystal and electronic band structure of Cu_2ZnSnX_4 (X = S and Se) photovoltaic absorbers: First-principles insights*". Appl. Phys. Lett. 94; 041903 (1-3); **2009.**

[53] C Perrson. "*Electronic and optical properties of Cu_2ZnSnS_4 and $Cu_2ZnSnSe_4$*". J. Appl. Phys. 107; 053710 (1-8); **2010.**

[54] TK Todorov, KB Reuter, DB Mitzi. "*High-Efficiency Solar Cell with Earth-Abundant Liquid-Processed Absorber*". Adv. Mater. 22; E156-E159; **2010.**

[55] H Katagiri, K Jimbo, S Yamada, T Kamimura, WS Maw, T Fukano, T Ito, T Motohiro. "*Enhanced Conversion Efficiencies of Cu2ZnSnS4-Based Thin Film Solar Cells by Using Preferential Etching Technique*". Appl. Phys. Exp. 1; 041201 (1-2); **2008.**

[56] K Wang, O Gunawan, T Todorov, B Shin, SJ Chey, NA Bojarczuk, D Mitzi, S Guha. "*Thermally evaporated Cu_2ZnSnS_4 solar cells*". Appl. Phys. Lett. 97; 143508 (1-3); **2010.**

[57] JJ Scragg, PJ Dale, LM Peter. "*Synthesis and characterization of Cu_2ZnSnS_4 absorber layers by an electrodeposition-annealing route*". Thin Solid Films 517; 2481–2484; **2009.**

[58] H Araki, Y Kubo, K Jimbo, WS Maw, H Katagiri, M Yamazaki, K Oishi, A Takeuchi. "*Preparation of Cu_2ZnSnS_4 thin films by sulfurization of co-electroplated Cu-Zn-Sn precursors*" Phys. Status Solidi C6 (5); 1266–1268; **2009.**

[59] S Chen, XG Gong, A Walsh, S-H Wei. "*Defect physics of the kesterite thin-film solar cell absorber Cu_2ZnSnS_4*". Appl. Phys. Lett. 96; 021902 (1-3); **2010.**

[60] SB Zhang, S-H Wei, A Zunger, HK-Yoshida. "*Defect physics of the $CuInSe_2$ chalcopyrite semiconductor*" Phys. Rev. B 57 (16); 9642-9656; **1998.**

[61] A Nagoya, R Asahi, R Wahl, G Kresse. "*Defect formation and phase stability of Cu_2ZnSnS_4 photovoltaic material*". Phys. Rev. B 81; 113202 (1-4); **2010.**

[62] S Chen, J-H Yang, XG Gong, A Walsh, S-H Wei. "*Intrinsic point defects and complexes in the quaternary kesterite semiconductor Cu_2ZnSnS_4*". Phys. Rev. B 81; 245204 (1-10); **2010.**

Chapter 3

Description and relevance of AMPS-1D for thin film photovoltaic modeling

This Chapter identifies the need for numerical modeling of tin-based heterostructures using a simulation tool called Analysis of Electronic and Photonic Structures – 1Dimensional (AMPS-1D), developed by Stephen Fonash and collaborators at the Pennsylvania State University, under the support of the Electric Power Research Institute (EPRI), and explains the functioning of the software. The underlying physical equations that govern photovoltaic (PV) behavior in such structures have been discussed along with the approach that the tool uses to solve a system of non-linear coupled differential equations. The salient features and advantages of this software over other similar tools in understanding device performances in terms of charge transport phenomena have also been listed.

3.1 The need for numerical modeling

The conclusion from the earlier two Chapters is that there is a growing need for alternative absorber materials that can yield superior conversion efficiencies at reduced material and production costs, and that the tin-based absorber system (both SnS and CZTS) has excellent potential by virtue of their favorable material properties and the long-term projected availabilities of the constituent materials. It has also been discussed in Chapter 2 that this material system is still in the early stages of research for PV device development, with few attempts at synthesis and physical characterization of tin-based junctions that represent the core of such cells. Given the long time frames (>30 years) over which the incumbent thin film technologies based on CdTe and CIGS have developed from their initial research studies to the present efficiency levels, it would be time consuming and disadvantageous in the current scenario to arbitrarily experiment with many materials for the different layers of a thin film

stack in the hope of getting to 20% efficiencies. It would instead be a smarter option if a basis for the effectiveness of tin-based PV devices with respect to energy conversion could be established and efficiency limits from using different materials quantified. This basis can be compared with the knowledge that has been gained and established from the two mature technologies to narrow the choice of materials and thereby channelize further research efforts in tin PV. The basis can be generated through theoretical studies such as models that account for all physical properties and device characteristics under different design configurations with respect to the incident light radiation. AMPS is a software that has been developed to solve the system of highly complex and non-linear equations that characterize a PV device under different operating conditions (thermodynamic equilibrium, light bias, etc.). This research uses AMPS to evaluate conversion efficiencies in tin-based PV systems for different materials and device configurations so that future research attempts at optimal device development can be better directed.

Figure 3.1 shows the interdependent and interdisciplinary nature of PV device development from the materials selection step (A) to the final stage of technology commercialization (G). The dashed rectangle indicates the scope of this research.

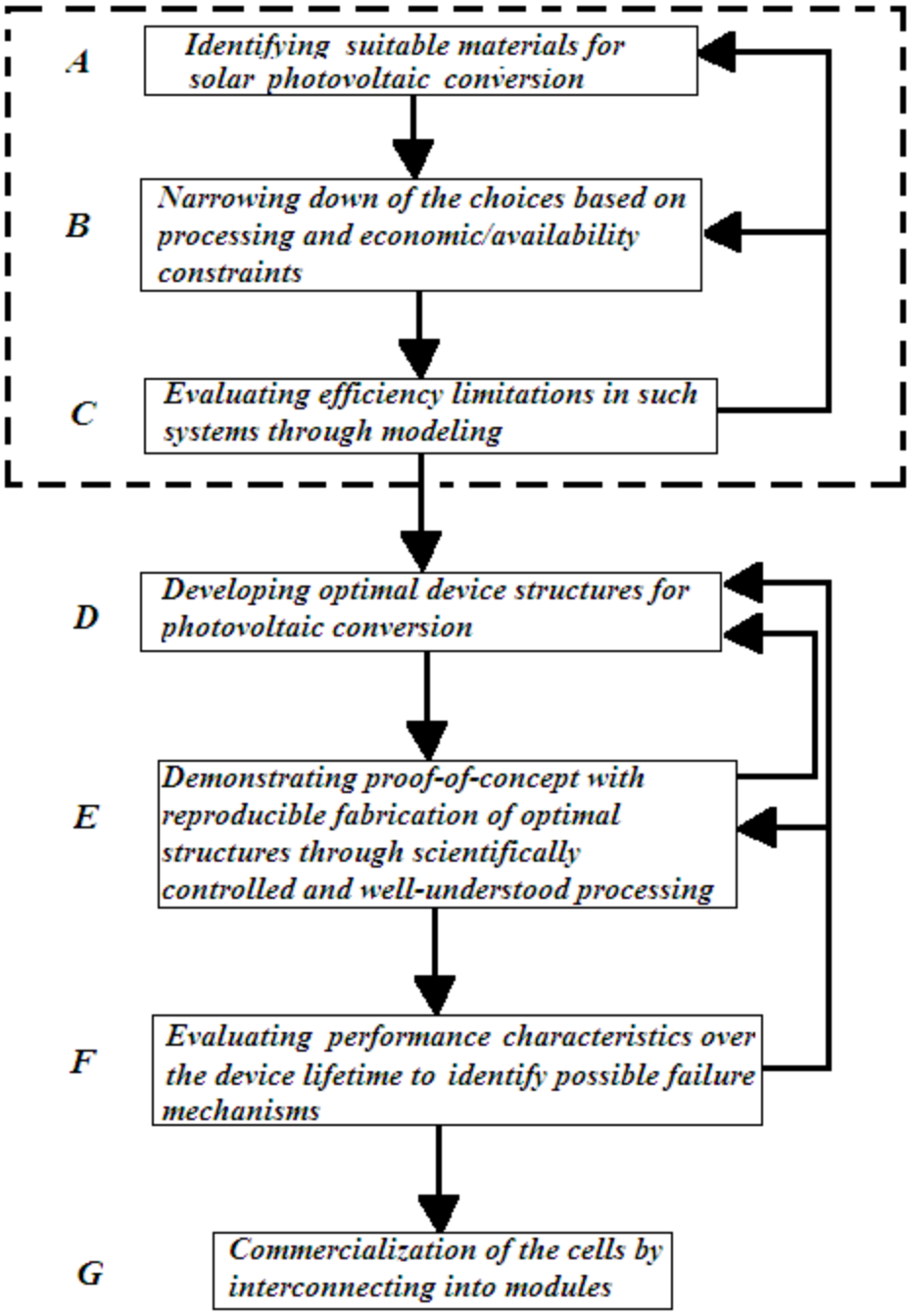

Figure 3.1: A flowchart illustrating the different stages of PV device development.

3.2 AMPS-1D: A description

AMPS is a very general computer program that has been developed for simulating one-dimensional transport physics in solid state devices. It uses the first-principles continuity and Poisson's equations approach to analyze the transport behavior of semiconductor electronic and optoelectronic device structures. AMPS may be used to examine a variety of device structures that include homojunction and heterojunction p-n and p-i-n, solar cells, multi-junction solar cell structures, novel device photovoltaic and opto-electronic structures, and Schottky barrier devices with optional back layers.[1,2]

3.2.1 The user interface and modeling inputs

In AMPS, each device system that is simulated is referred to as a 'case'. Figure 3.2 shows the main panel that lists all the material parameters required of the different layers and the incident light spectrum. Note that there are two modeling approaches permissible in AMPS, namely the lifetime picture and the Density of States (DOS) model. The former assumes a linearized kinetic model of only the band-to-band transition process in terms of the photogenerated charge carrier lifetimes, whereas the latter fully accounts for the indirect (gap state-assisted) recombination and charge trapping permissible in these structures.[1] All models developed in this dissertation adopt the DOS approach, as evident from the button selection shown in Figure 3.2.

Figure 3.3 shows the different optoelectronic properties and material thickness that the program requires of the different layers that constitute a thin film PV device. The material parameters denoted at the bottom are dielectric permittivity (EPS), electron and hole mobilities (MUN and MUP), native acceptor and/or donor carrier concentrations (NA and ND), optical band gap (EG), effective density of states of valence and conduction band edges (NV and NC), and electron affinity (CHI). The Center grid spacing is a user choice that denotes the space interval between two points of simulation, and

must be selected such that the total number of grid points across the entire thickness of the device does not exceed 500.[1] The optoelectronic properties of all the materials used in this dissertation have been listed in Appendix B for reference.

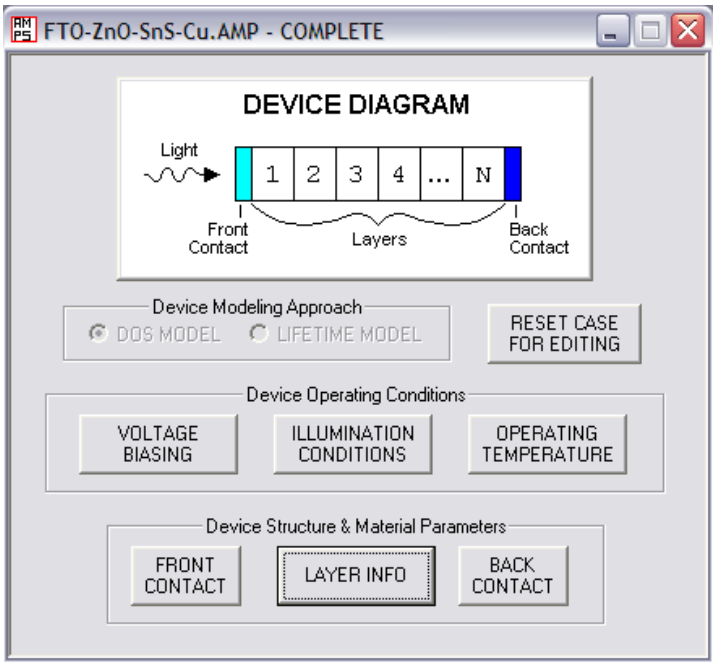

Figure 3.2: A snapshot of the AMPS interface showing all the required parameters.

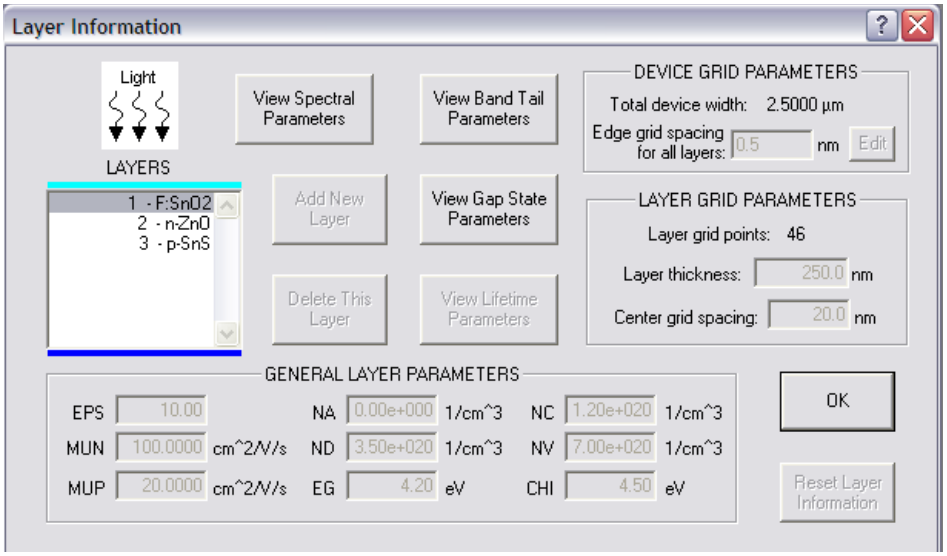

Figure 3.3: The optoelectronic properties of the different material layers required as input in AMPS.

Figure 3.3 also shows that the software permits input of band tail and gap state parameters that account for charge behavior in the forbidden energy gap. This dissertation assumes discrete conduction and valence band edges for all the material layers, implying no donor- or acceptor-like tail states that extend into the band gap and contribute to charge conduction. The objective of this research is to only model baseline tin-based heterostructures, which means that no intermediate gap states having discrete or Gaussian distribution of energy levels are considered or assumed. It should be mentioned that there is little prior experimental evidence or information on the defects and/or dopants possible in the tin-based absorber, and their role in promoting or inhibiting photogenerated charge transport has not yet been understood.

All simulations performed in this dissertation correspond to a constant cell operating temperature of 300K (ambient temperature). Since the focus of this work is to study the performance of optoelectronic structures under illumination, no voltage biasing (cf. Figure 3.2) has been considered or its influence evaluated.

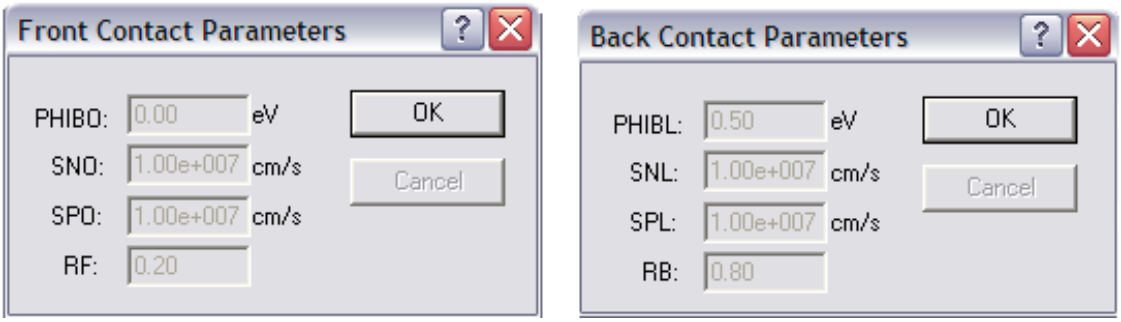

Figure 3.4: Parameters that define the contacts that separate and collect the photogenerated electrons and holes at the respective ends of the PV device. Refer to Appendix A for definition of 'Front' and 'Back' relative to AMPS convention.

The photogenerated (and separated) electrons and holes in the PV device are separated at opposite ends using suitable contacts having high electrical conductivities that promote charge transport. The

contacts referred to in Figure 3.4 are not considered a part of the main AMPS structure and that their thickness is not a physical consideration affecting PV action. The parameters PHIBO and PHIBL, therefore, correspond to the barrier heights encountered by the charge carriers at x=0 (front surface) and x=L (back end), respectively, and are always defined numerically as (E_c-E_F), where E_c refers to the conduction band edge energy level of the adjoining material at the electrochemical junction (i.e. at $x=0^+$ or L^-) and E_F is the fermi level of the contact material relative to the local vacuum energy level. The parameters SN and SP refer to surface recombination speeds (at x=0 and x=L) that typically have values ~10^7 cm/s to account for the quality of interface in the form of dangling bonds, adsorbed species, and other impurities arising from experimental conditions. The parameters RF and RB represent the optical reflection coefficients of the front and back interfaces, respectively, and indicate the fraction of irradiance that is reflected off the surface and hence not contributing to charge generation and separation.

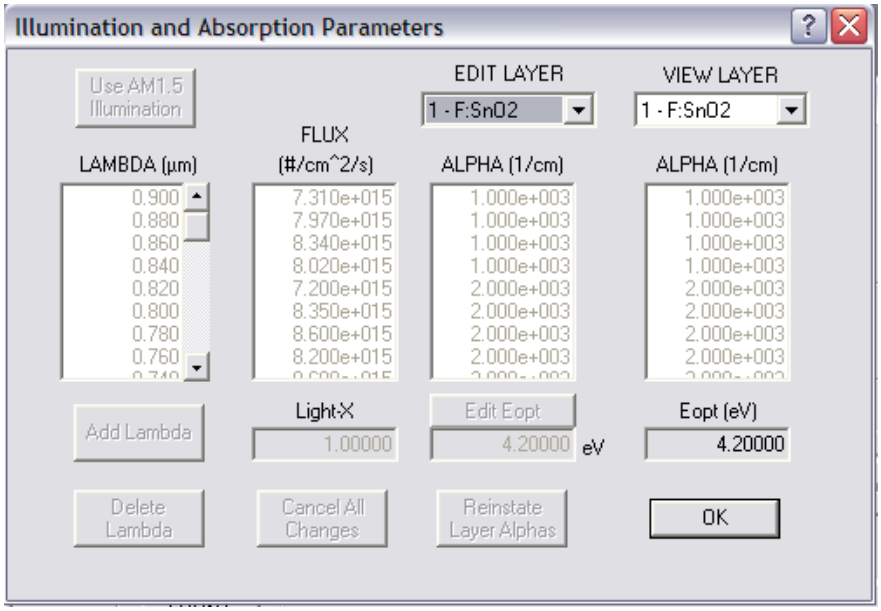

Figure 3.5: The illumination and absorption parameters used in AMPS modeling.

Figure 3.5 shows the material parameters required by AMPS to fully describe the type and role of irradiance on photoabsorption by the different layers of a PV cell. All simulations have been carried

out under AM1.5G illumination that represents the typical average terrestrial irradiance. In AMPS the selection of the AM1.5 illumination button at the top left of Figure 3.5 automatically inputs the visible band region (380-900 nm) along with the corresponding photon flux intensities for each 20 nm bandwidth that together represent the irradiance spectrum, the nature of which is explained in Chapter 1. ALPHA refers to the absorption coefficient profile of each material layer in the device, and must be manually entered based on deductions from experimental results and calculations. The absorption profiles of all the materials used in this dissertation have been listed in Appendix C for reference.

3.2.2 The governing equations

The physics of device transport can be explained by the three underlying equations: Poisson's equation, the continuity equation for free holes, and the continuity equation for free electrons.[1] Poisson's equation links free carrier populations, trapped charge populations, and ionized dopant populations to the electrostatic field present in a material system. In one-dimensional space, Poisson's equation is given by: [1]

$$d/dx\left(-\varepsilon(x)\frac{d\psi}{dx}\right)=q\times\left[p(x)-n(x)+N^{+}{}_{D}(x)-N^{-}{}_{A}(x)+p_{t}(x)-n_{t}(x)\right] \qquad \text{Eq. (3.1)}$$

where the electrostatic potential ψ and the free electron n, free hole p, trapped electron n_t, and trapped hole p_t, as well as the ionized donor-like doping N_D^+ and ionized acceptor-like doping N_A^- concentrations are all given in terms of the different band energy levels by the Fermi-Dirac and Boltzmann distributions, and vary with the position coordinate '*x*'.[1] The coordinate '*x*' is always measured positively from the illuminated end and represents the position of the device cross section (which is a plane normal to the impinging light radiation) at any point along the thickness of the device. Here, ε is the material permittivity and q is the magnitude of the charge of an electron. In this work, full ionization is assumed for all layers i.e. $N_A = N_A^-$ or $N_D = N_D^+$, depending on whether the material is p- or n-type, respectively.

The continuity equations describe the variation in free carrier populations in the respective delocalized bands of the different material layers across the thickness of a device under illumination. Under steady-state i.e. when the time-rate of change of free carrier populations is zero, these equations can be described as: [1]

$$\frac{1}{q}\left(dJ_n/dx\right) = -G_{op}(x) + R(x) \quad \text{for free electrons} \qquad \text{Eq. (3.2)}$$

and

$$\frac{1}{q}\left(dJ_p/dx\right) = G_{op}(x) + R(x) \quad \text{for free holes} \qquad \text{Eq. (3.3)}$$

where J_n and J_p are, respectively, the electron and hole current densities. The term $R(x)$ is the total recombination rate accounting for band-to-band (direct) and Shockley-Reed-Hall (indirect) recombination traffics. The term $G_{op}(x)$ refers to the optical carrier generation rate as a function of position '*x*' due to illumination. It is defined and computed at each point as the spatial derivative of the incident photon flux Φ_i that is a function of frequency 'ν' and has standard values ($\sim 10^{15}/cm^2/s$) for the AM1.5 spectrum at 20 nm bandwidth intervals. It is noted that as the photon flux travels through the structure, the rate at which electron-hole pairs are generated is proportional to the rate at which the photon flux decreases.

The direct (or radiative) recombination process is relatively simple to account for because it only involves the occupied states in the conduction band and the vacant states in the valence band, so that the recombination rate is directly proportional to the product of the free carrier populations, n•p, at every point '*x*' in the device.[1] However, the indirect recombination process is highly complex as it involves charge transitions between the delocalized bands and the localized gap states that can be banded and/or discrete due to dopants (purposefully added) or traps (structural defects and impurities) residing in these energy levels. AMPS calculates this recombination rate in terms of the defect energy

level distribution (that may be manually input) and the probability of charge carriers to be trapped in these states (given by Fermi distribution).[1]

3.2.3 Solving the equations

The three governing equations (3.1), (3.2), and (3.3) must hold at every position in a device and the solution to these equations involves determining the state variables $\psi(x)$, $Ef_n(x)$, and $Ef_p(x)$ or, equivalently, $\psi(x)$, $n(x)$, and $p(x)$ which completely defines the system at every point *x*. Because the governing equations for the three variables are non-linear and coupled, numerical methods must be utilized to discretize the differential equations in order to solve them.[1]

To discretize the differential equations the method of finite differences is utilized.[1]

$$\frac{d^2\Psi(x_i)}{dx^2} = \frac{\Psi x_{i+1} - 2\Psi x_i + \Psi x_{i-1}}{h+H} \qquad \text{Eq. (3.4)}$$

where h is the backward distance between adjacent grid points and H is the forward distance between adjacent grid points in the device.

$$\left[\frac{dJ_p}{dx}\right]_i = \frac{J_{p_{i+1/2}} - J_{p_{i-1/2}}}{h+H}$$ for the hole continuity equation Eq. (3.5)

$$\left[\frac{dJ_n}{dx}\right]_i = \frac{J_{n_{i+1/2}} + J_{n_{i-1/2}}}{h+H}$$ for the electron continuity equation Eq. (3.6)

Once the state variables ψ, E_{fn}, and E_{fp} are determined for a given set of biasing conditions (such as light) and temperatures, the current density-voltage (J-V) characteristics for these conditions can be generated. The J-V characteristic for some temperature T, with or without the presence of light, is obtained from the fact that $J=J_p(x) + J_n(x)$ for any point '*x*' in the device.

3.2.4 The output variables in AMPS

AMPS computes and provides a graphical representation of a number of physical variables as a function of the position coordinate '*x*' that can be ultimately used based on our understanding to explain physical features and quantify their influence on the simulated J-V characteristics. Figure 3.6 shows an image of the output window wherein the list of variables are displayed and can be selected to view as plots or data. AMPS can also be used to study the change in values of a variable under no light bias (i.e. thermodynamic equilibrium) and upon illumination, at the three operating conditions, short-circuit current density, open-circuit voltage, and maximum power point. It can also be seen from Figure 3.6 that AMPS permits simultaneous plots of multiple cases to compare and explain PV behavior in different device schemes.

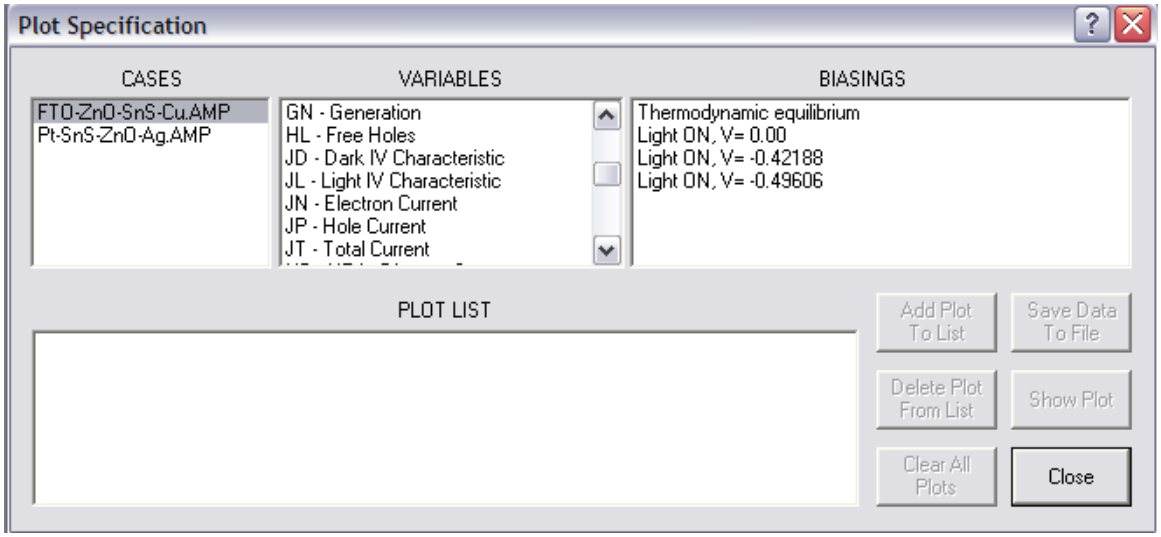

Figure 3.6: The output window in AMPS-1D showing a partial listing of the physical variables.

3.3 Salient features of AMPS-1D

The uniqueness of AMPS lies in its ability to examine a variety of device structures such as:[1]

- homojunction and heterojunction p-n and p-i-n, solar cells and detectors;

- multi-junction solar cell structures;
- novel device photovoltaic and optoelectronic structures;
- Schottky barrier devices with optional back layers

Though other programs such as Solar Cell Capacitance Simulator in 1 Dimension (SCAPS-1D) and PISCES have been developed to analyze electronic devices, AMPS is the only software that incorporates all recombination and defect charge distribution mechanisms on a spatially varying scale for multiple layers (upto 30).[3] This explains the fact that AMPS is the most robust tool in terms of its ability to numerically converge a wide variety of device systems,[3] which is important when comparing multiple materials as is the case in this research. The major disadvantages of AMPS are direct tunneling is not incorporated and its speed is slow compared to other programs.[3]

References

[1] J Arch, J Hou, W Howland, P McElheny, A Moquin, M Rogosky, F Rubinelli, T Tran, H Zhu, SJ Fonash. "*A Manual for AMPS 1-D BETA Version 1.00*". **1997**.

[2] SJ Fonash. Solar Cell Device Physics. 2nd edition Elsevier USA, **2010**.

[3] M Burgelman, J Verschraegen, S Degrave, P Nollet. "*Modeling Thin-film PV Devices*". Prog. PV: Res. Appl. 11; 1–11; **2003**.

Chapter 4

Evaluating photovoltaic conversion efficiencies in CdTe and SnS-based devices

In this Chapter, a comparison of numerical models developed for baseline devices utilizing tin monosulfide (SnS) and CdTe as the absorbing materials and based on three n-p heterojunctions (HJ) has been made to reveal PV conversion efficiencies under AM1.5 illumination. Charge transport across the junction formed between selected light absorbers (p) and light-transmitting window materials (n-CdS or n-ZnO) has been studied by modeling the configurations relative to the incidence of light: the *window-absorber* design is described in this Chapter. The goal of this study is to identify avenues for efficiency improvements in SnS PV device design relative to the CdTe system based on increases in either short-circuit current densities or open-circuit voltages, or both. This study also reveals the most promising material scheme for achieving higher than 20% efficiencies in tin-based PV.

4.1 Materials selection and properties

The two window materials considered for n-p heterojunction (HJ) formation with the absorber materials are CdS and ZnO (for a description of window materials, please refer to Appendix A). The former is considered because of our familiarity with its optoelectronic behavior as part of a PV stack, while the latter offers easier processing capabilities and has a better suited band gap (3.35eV) for supporting PV action. The two p-type absorber materials (designated simply “absorber”) in this study are CdTe and SnS. The former is well known in commercially available thin film PV devices, while the latter has been emerging in the laboratory as a possible alternative due to favorable optoelectronic properties and favorable economic positioning in the material supply chain.

The optoelectronic properties of the different material layers used in this study have been taken from Gloeckler's baseline paper on thin film PV systems.[3] The optoelectronic properties for SnS such as free carrier concentration and density of states were used from B. Subramanian et. al's paper,[4] while the absorption profile was calculated from the work of Brownson et. al.[5] The values of the different parameters used in the models can be found in Appendix B and the absorption profiles are listed as a function of wavelength λ in Appendix C.

The band gap of CdS is low enough (2.4 eV) for the high-energy violet region of the AM1.5 solar spectrum to be absorbed by the window material, so that fewer photons are available for the absorber layer for generating electron-hole pairs. The wider band gap ZnO (3.35 eV) has therefore been considered and modeled as an alternative Schottky barrier material to CdS in this study keeping all other device parameters constant. For similar reasons, ITO has also been replaced with FTO as the transparent conductive oxide (TCO) material that is interfacing the front surface of the oxide layer.

4.1.1 Device structures

Figure 3.2 describes the different layers that are part of a PV device model and the conventions used in this study. Note that in all AMPS plots light is incident from the left end and distances '*x*' are measured from this surface (more on conventions in Appendix A). The hole collector used in the rear end is usually a metal (such as copper, in this study), and is not a part of the main device structure. AMPS calculates all potentials relative to the reference vacuum level at the right end of the cell and current flow is defined positive in the direction shown in Figure 3.2.[6] It should be evident from Figure 3.2 that the flow of higher energy conduction electrons from the left (illuminated) end to the right (dark) indicates higher potentials at the illumination side for such devices. However, per AMPS convention, voltages are all calculated from the right end, and resulting J-V plots can occur in the second quadrant instead of the normally encountered first quadrant.

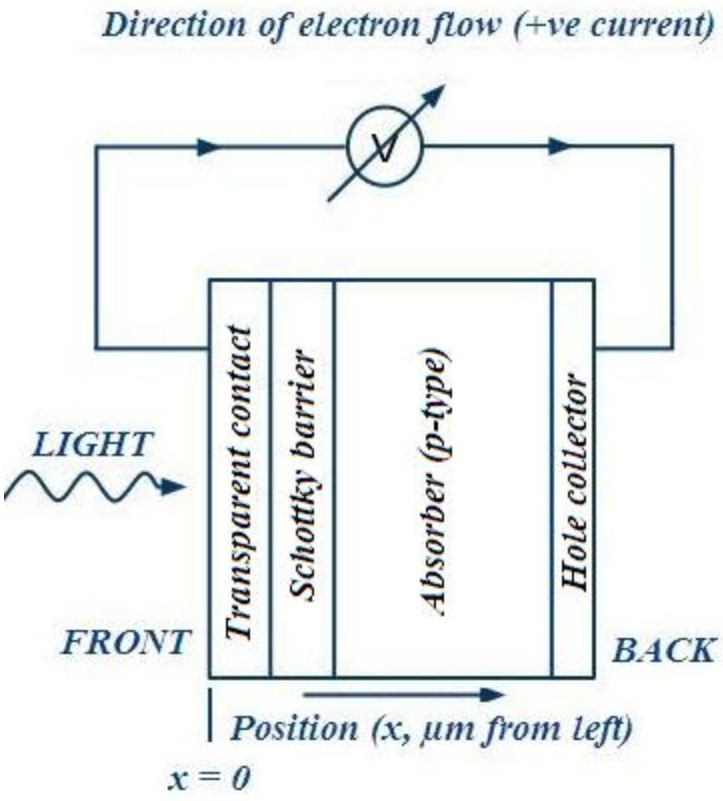

Figure 4.1: Typical schematic of thin-film PV devices modeled in AMPS-1D.

In this research, the skeletal structure of the most typical devices based on CdTe has been modeled. These devices utilize 0.2 μm In_2O_3-SnO_2 (ITO) as the TCO, on which a 0.2 μm layer of CdS (wide band gap) serves as the window material that forms the Schottky barrier with the 5 μm-thick absorber CdTe (cf. Figure 4.1). Copper has been used as the metal forming the ohmic contact at the rear end, and its thickness is not a consideration that affects PV behavior. This device [0.2 μm ITO|0.2 μm CdS|5 μm CdTe| Cu] is compared with similar structures based on SnS to quantify PV conversion efficiencies in the two absorber systems and identify avenues for further improvements in the latter. The two SnS-based devices that have been modeled have the configurations 0.25 μm ITO| 0.25 μm CdS| 2 μm SnS| Cu (*oxide-absorber*) and 0.25 μm F-doped SnO_2 (FTO)| 0.25 μm ZnO| 2 μm SnS| Cu (*absorber-oxide*).

4.2 Results and discussion

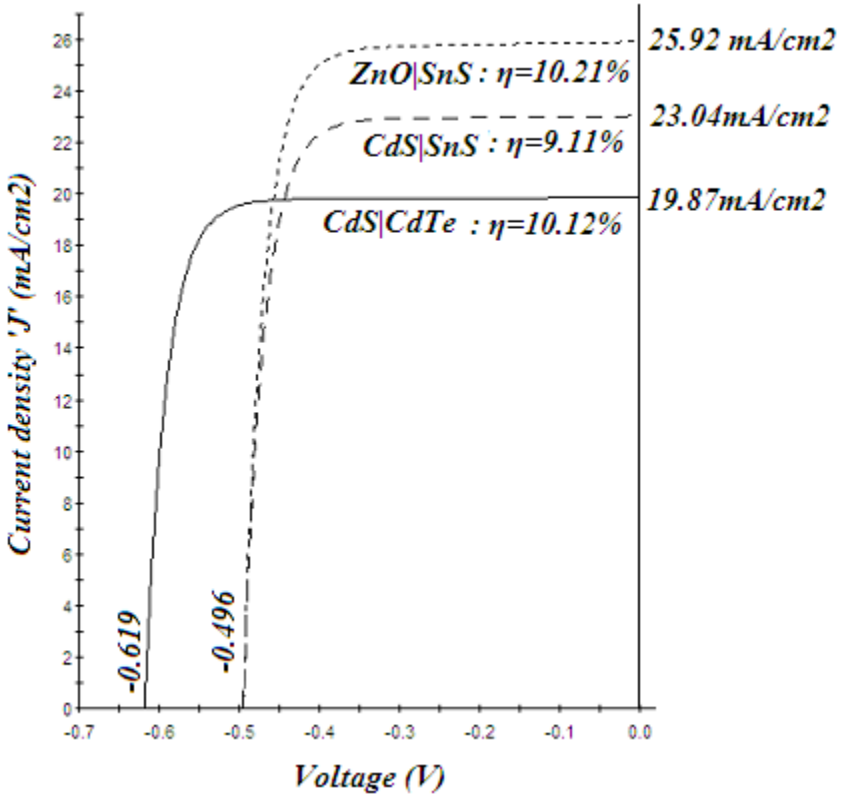

Figure 4.2: J-V characteristics of the three illuminated PV systems: CdS|CdTe (solid), CdS|SnS (dashed) and ZnO|SnS (dotted).

Figure 4.2 displays the simulated J-V characteristic under illumination, revealing that the model predicts short-circuit current densities J_{sc} (19.87 mA/cm^2) and open-circuit voltages (0.619 V) that correspond to a conversion efficiency of 10.12% for the CdS|CdTe system. The CdTe band gap (E_g) is 1.5 eV; however the performance shows a higher voltage deficit of 0.881 V, suggesting unfavorable thermodynamic band alignments at the right (dark) ohmic contact for majority carrier transport.

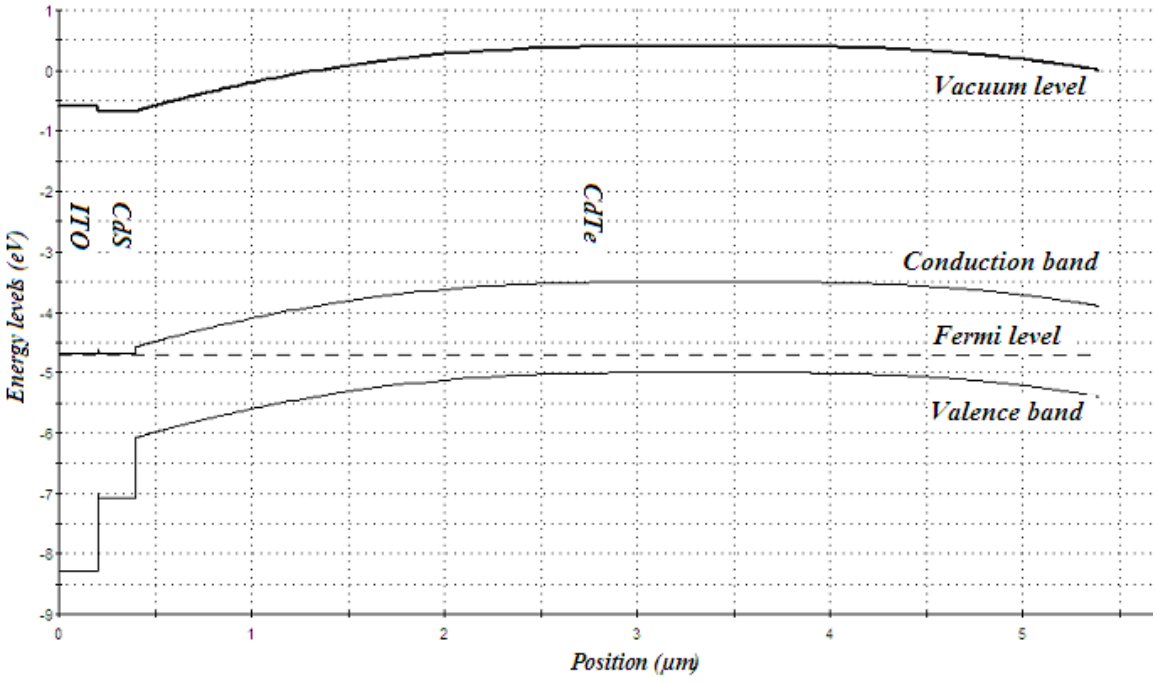

Figure 4.3: Energy band diagram of the ITO|CdS|CdTe|Cu PV device under thermodynamic equilibrium (no light).

Figure 4.3 further illustrates a 0.4 eV potential drop under equilibrium near the back surface of the absorber between 4-5.4 μm that causes narrowing of the quasi-fermi level splitting of photogenerated electrons and holes in CdTe and results in low open-circuit voltage predictions for the device.

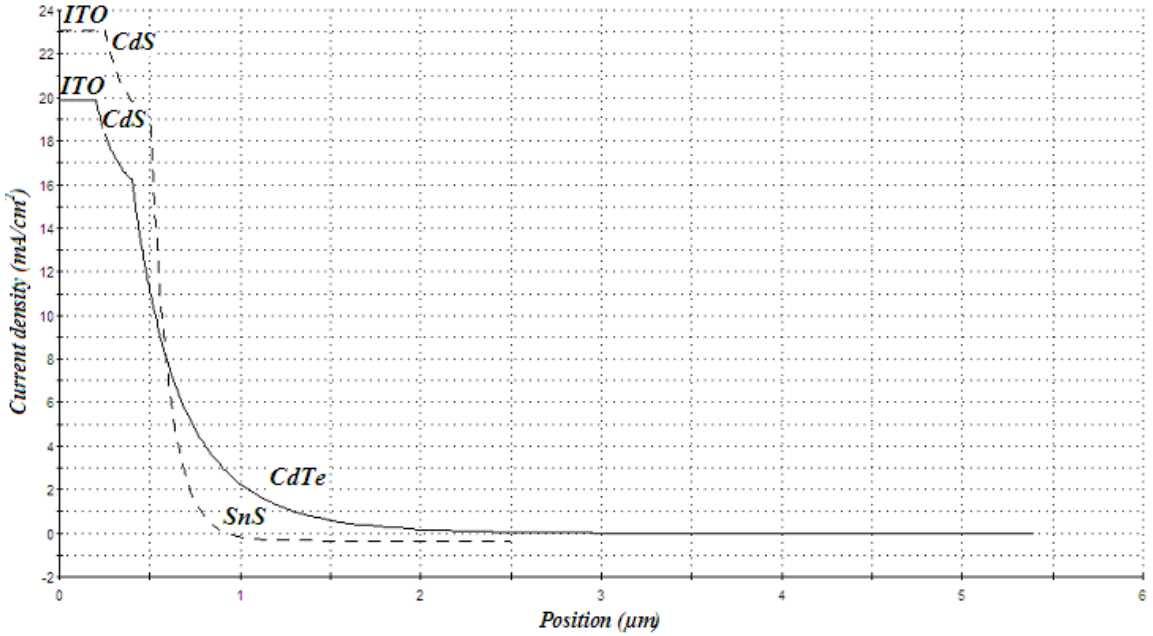

Figure 4.4: Variation of short-circuit electron current density across the thickness of the illuminated CdS|CdTe (solid) and CdS|SnS (dashed) devices.

Figure 4.2 also shows a comparison of the predicted short-circuit current densities for the CdS|SnS and CdS|CdTe device schemes, indicating higher values (by 3.2 mA/cm^2) for the former. Noting that the total current across the device is constant and its value is numerically limited by the sum of the minority carrier current contributions on either side of the n-p HJ, the magnitude of electron current in the p-type absorber at the electrochemical junction with CdS is the distinguishing factor influencing current densities in the two systems.

Figure 4.4 shows electron currents of 16.2 and 19.1mA/cm^2 at the electrochemical junction under short-circuit for the CdS|CdTe (x=0.4 μm) and CdS|SnS (x=0.5 μm) devices respectively. This difference (2.9 mA/cm^2) accounts for the 3.2 mA/cm^2 superiority (Figure 4.2) in SnS-based devices. However, the electron current becomes slightly negative beyond x=0.9 μm in SnS (cf. Figure 4.4), which suggests reversal of current flow, actually consuming power in proportion to the negative

current density of 0.3mA/cm^2. The sum of positive and negative current contributions still offers superior performance from SnS-based devices: 2.9 mA/cm^2.

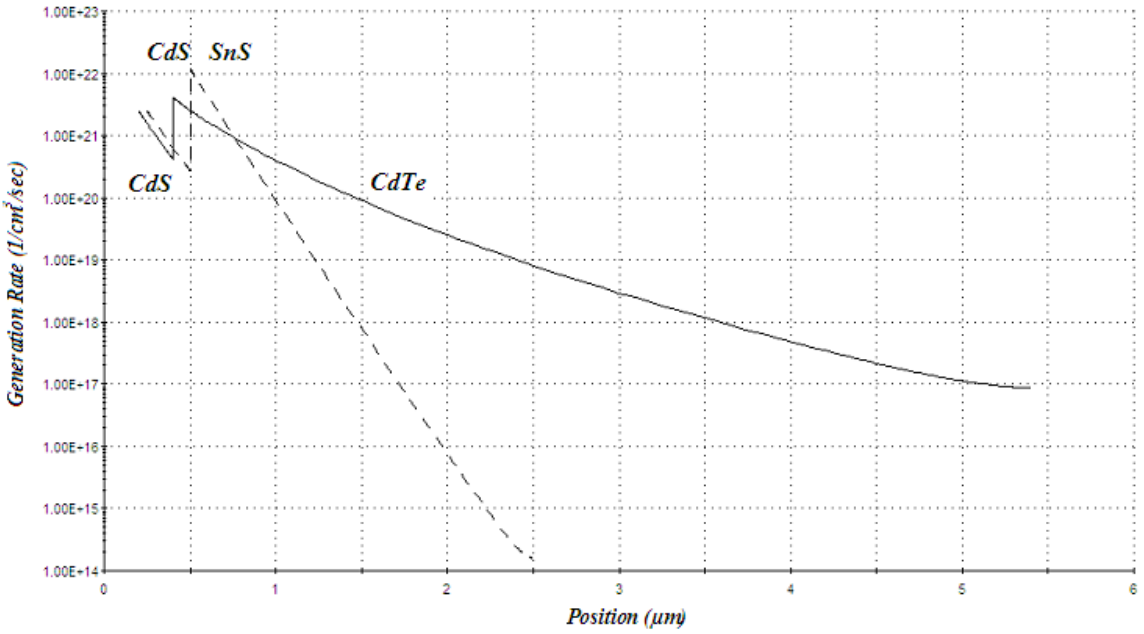

Figure 4.5: Spatial variation in electron generation rates for the CdTe (solid) and SnS (dashed)-based PV devices upon illumination (semi-log plot).

Figure 4.5 displays the difference in minority currents for the two absorber layers, explained in terms of their electron generation rates upon optical absorption. The electron current density at any point 'x' in the absorber is given based on the transport theory by [3]:

$$J_n = q\mu_n n\left(dE_{fn}/dx\right) \qquad \text{Eq. (3.7)}$$

where μ_n is the electron mobility, n is the conduction band electron population, E_{fn} is the electron quasi-fermi level at steady-state upon illumination, and q is the electronic charge. Both the quantities 'n' and 'dE_{fn}/dx' are in turn directly related to the optical generation rate $G_{op}(x)$, which is defined and computed in AMPS as the spatial derivative of the total optical flux intensity at the point 'x'.

An inspection of the photogenerated electron rate distribution in Figure 4.4 suggests higher minority carrier generation rates in SnS compared to CdTe (by a factor of three) at the front n-p metallurgical junction, which contributes to higher free electron populations and explains the greater minority current densities in the space charge region of the tin absorber. The greater absorption in SnS at the n-p electrochemical junction is also responsible for the sharper decline in carrier generation rates observed in this material (cf. Figure 4.5) relative to CdTe, since a greater fraction of the high energy photons are absorbed closer to the left end before they traverse its thickness. The higher photogenerated carrier rates in SnS compared to CdTe are a direct consequence of its lower band gap (1.25 eV vs. 1.5 eV), which permits increased absorption of the incident AM1.5G spectrum.

Figure 4.2 also indicates lower open-circuit voltages (V_{oc}) for the tin-based system, attributable again to the lower absorber band gap. However, the voltage deficits in SnS PV are only 0.754 V compared to 0.881V for CdTe, and can be explained by the smaller free carrier densities in the latter (7.4×10^{16} cm^{-3} for SnS compared to 2×10^{14} cm^{-3} for CdTe) that create micron-thick depletion region (cf. Figure 4.3) and result in higher bulk recombination. Since V_{oc} is theoretically governed by the difference between the split electron and hole quasi-fermi levels, i.e.,

$$Voc = 1/q \cdot (Efn - Efp) \qquad \text{Eq. (3.8)}$$

increase in recombination rates narrow the splitting in the absorber upon illumination and thus reduce voltages.

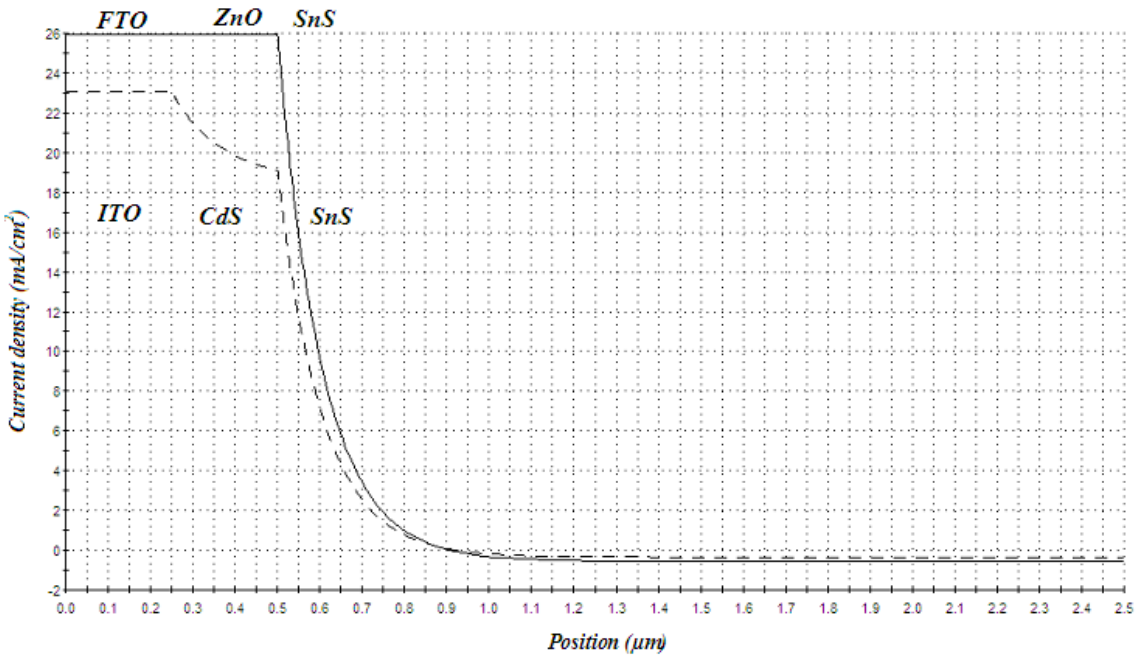

Figure 4.6: Spatial variation in short-circuit electron current densities in *oxide-absorber* (solid) and *sulfide-absorber* (dashed) devices upon illumination.

As stated, the absorption of higher energy wavelengths by CdS causes significant drop in short-circuit current densities for CdS|SnS devices (herein referred to as the *sulfide-absorber*), and suggests the use of wider band gap ZnO for higher cell efficiencies. It can be seen in Figure 4.2 that an increase in short-circuit current density of 2.88 mA/cm^2 can be observed by using the oxide as the window material instead of the sulfide. It is also noted that the open-circuit voltage is not changed between the two SnS device schemes because of their identical back contact barrier heights that most critically influence fermi level splitting in the absorber upon illumination.

The higher currents in *oxide-absorber* are due to the increased photoabsorption and generation in the absorber at the n-p HJ that determines the magnitude of the overall device current. Note that in Figure 4.6, electrons completely dominate the overall current crossing the HJ (x=0.5μm) in the oxide cells, whereas holes constitute a fraction of the total current in *sulfide-absorber* devices at this plane, the magnitude of which is equal to the reduction in electron current across CdS thickness. This

phenomenon is due to absorption/generation followed by recombination of electron-hole pairs in the window layer that results in fewer photons available for absorption by SnS, and thus lower overall currents in CdS-based structures.

4.3 Summary

A comparison of the three device systems (cf. Figure 4.1) indicates remarkably similar PV conversion efficiency values for the CdS|CdTe and ZnO|SnS systems (>10%), with a 1 percentage-point reduction for CdS|SnS cells. The higher current densities predicted in *oxide-absorber* based cells is compensated by greater open-circuit voltages for the CdTe-based device by virtue of its wider band gap. However, a comparison of the V_{oc} values with the respective band gaps suggests smaller voltage deficits in SnS due to their higher free carrier concentrations that permit smaller space charge regions and wider fermi level splitting due to reduced bulk recombination. It is therefore expected that increasing the voltages in *oxide-absorber* based devices could be the best way forward for thin film PV to break the 20% efficiency wall. Two research directions may be considered in this regard, one on identifying and modeling superior back contact materials and cell architectures that permit cost-effective and efficient PV conversion, and another on increasing the optical band gap of the chalcogenide closer to the ideal value (1.5eV) by lattice dissolution and modification into CZTS (Cu-Zn-Sn-S).

With CdTe-based PV constrained in efficiency improvements due to the difficulty in finding suitable metals that can form chemically stable rear ohmic contacts for efficient majority carrier transport, the tin-suite of materials based on tin monosulfide (SnS) have been studied as the next generation of light absorbing materials that can potentially cross the 20% efficiency barrier in thin film PV. Numerical modeling using AMPS-1D predicts higher J-values of 23.04mA/cm^2 in CdS|SnS devices compared to CdS|CdTe (19.86mA/cm^2), an observation that is attributed to greater electron generation rates at the n-p HJ in case of SnS by virtue of its lower band gap. Due to absorption losses in CdS-based devices

ZnO is modeled as an alternative window layer, and this material promises enhanced current densities of 25.9mA/cm^2. Though SnS-based PV offers lower open-circuit voltages (0.496V) with respect to CdTe (0.619V) that compensate the higher current densities in such systems, the voltage deficits in the tin-based absorber are lower and suggest scope for efficiency improvements through band gap modifications by alloying, analogous to CIGS (Cu-In-Ga-S).

References

[1] J Arch, J Hou, W Howland, P McElheny, A Moquin, M Rogosky, F Rubinelli, T Tran, H Zhu, SJ Fonash. "*A Manual for AMPS 1-D BETA Version 1.00*". **1997**.

[2] M Burgelman, J Verschraegen, S Degrave, P Nollet. "*Modeling Thin-film PV Devices*". Prog. PV: Res. Appl. 11; 1–11; **2003**.

[3] M Gloeckler, AL Fahrenbruch, JR Sites. "*Numerical Modeling of CIGS and CdTe Solar Cells: Setting the Baseline",* 3rd conf. on PV energy conv.; 491-494; **2003**.

[4] B **Subramanian, C Sanjeeviraja, M Jayachandran. "***Cathodic electrodeposition and analysis of SnS films for photoelectrochemical cells*". Mat.Chem. & Phys. 71; 40-46; **2001**.

[5] JRS Brownson, C Georges, CL-Clement. "*Synthesis of a δ-SnS Polymorph by Electrodeposition*". Chem. Mat. 18; 6397-6402; **2006**.

[6] SJ Fonash. Solar Cell Device Physics. 2nd edition Elsevier USA, **2010**.

Chapter 5

A case for 20%+ efficient cost-effective thin film photovoltaic devices based on SnS|ZnO heterojunctions

Chapter 4 suggested that ZnO|SnS based PV devices promised higher efficiencies compared to CdS|SnS cells by virtue of their superior light absorption characteristics that resulted in higher current densities. Devices based on the binary SnS (II-VI semiconductor) absorber have therefore been proposed and modeled in this Chapter to identify their potential for cost-effective photovoltaics. Charge transport across the p-n heterojunction formed between SnS (absorber) and ZnO (oxide) has been studied by modeling two different configurations relative to the incidence of light: the *absorber-oxide* design (where SnS is the front layer absorbing light first) and *oxide-absorber* design (reversed, where ZnO is the window layer). The two device schemes have been considered based on metrics of material requirements and expected performance challenges, and efficiency limits are predicted for such configurations.

5.1 Materials selection and properties

ZnO is considered as an excellent complement to SnS in this study because of its wide band gap (~3.35 eV), high free carrier concentrations for electron conduction (10^{18} cm^{-3}), and very similar electron affinity (4.35 eV) to SnS.[1] These properties suggest minimal voltage losses during charge transport across the interface. The oxide has been shown to form a chemically stable p-n heterojunction,[2] such that the photogenerated electrons (minority carriers) from the absorber can be collected effectively and transported to their respective contacts with minimal current losses. Also, the low toxicity and relatively easy processing of ZnO make it an attractive proposition for large-scale utilization with SnS.

In Figure 5.1 is shown a schematic of the two proposed devices, displayed with the front contacts (exposed to light) on the left side, and the rear contacts on the right, by AMPS convention. The devices will be hereafter termed the *oxide-absorber* heterojunction (ZnO|SnS; left in Figure 4.1) and the *absorber-oxide* heterojunction (SnS|ZnO; right in Figure 4.1) relative to the convention. In the *oxide-absorber* device, the ZnO serves as a "window" layer that transmits most of the visible band solar irradiance to the underlying SnS absorber material. In the alternative *absorber-oxide* device, the SnS absorbs the irradiance directly. As a result, the current densities predicted from the two devices have opposite signs, as indicated in Figure 4.1.

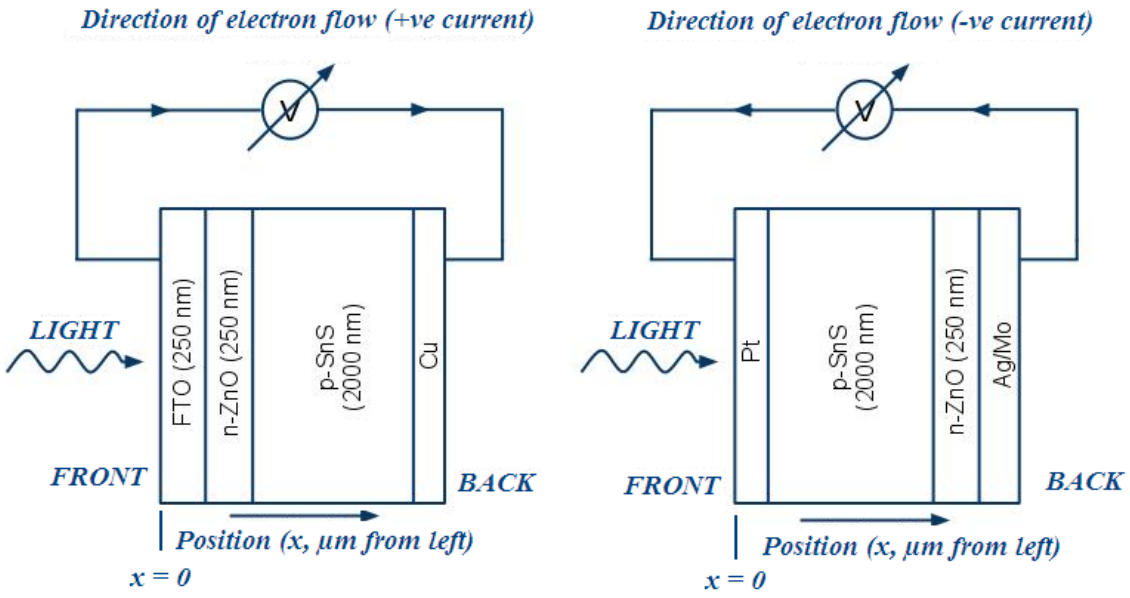

Figure 5.1: Schematic of the two modeled PV devices (light incident from left per AMPS standard) based on the interface between absorber (p-SnS) and oxide (n-ZnO). Left: the *oxide-absorber* heterojunction, right: the *absorber-oxide* heterojunction. The electrochemical junction at the p-n interface occurs at x=0.5µm (left) and 2µm (right).

It should be expected that the different material layers shown in Figure 4.1 are typically deposited on an inexpensive substrate such as glass to form a thin film stack based on either of the two configurations. This deposition scheme suggests that for the *oxide-absorber* configuration the ohmic

contact to the absorber would be initially deposited on glass followed by the 2 μm SnS layer, on top of which the 0.25 μm-thick ZnO is deposited to complete n-p HJ formation. To minimize optical absorption losses from the front ZnO surface by reflection and maximize collection of photogenerated electrons from the oxide, a 0.25 μm TCO layer of FTO is used as part of the model structure. In this layout, the rear metal contact (on glass) should be thick enough to withstand mechanical stresses caused by the overlaying materials so that the integrity of the absorber-contact interface is not compromised for PV performance over the course of the device lifetime. This requirement necessitates metal layer thicknesses greater than 0.5 μm, as is typically observed with Mo in CIGS-based cells. Since the ideal contact should have a work function higher than that of SnS (5.4 eV), the only metal satisfying this condition is platinum. Assuming metal layer thicknesses of 0.5 μm, the use of platinum would cost \$550/m^2 of module manufactured at 2010 metal prices.[3] The benchmark manufacturing costs of thin film PV cells are currently ~\$90/m^2 for CdTe,[4] and face continuous downward pressure to remain a sustainable source of cost-effective electricity. Such values clearly indicate that even if the amount of platinum used per cell were to be reduced through process improvements and better utilization rates by a factor of five (to 0.1 μm), the employment of this metal would still render such a PV technology economically unviable, however efficient it may be. The copper metal is therefore used as an alternative rear contact material because it is not only much less expensive but is also a more familiar material for thin film PV stacks.

For the *absorber-oxide* configuration (right in Figure 4.1), a layer of silver has been used to form ohmic contact to the overlying ZnO layer by virtue of its chemical stability and lower work functions in relation to the oxide. Platinum is shown as a thin film layer on top of SnS in the schematic, however it should be expected that metal fingers buried into the absorber (similar to c-Si cells) would be the most cost-effective means to minimize platinum use and absorption losses due to shadowing.

The optoelectronic properties of the different material layers used in this study have been taken from Gloeckler's baseline paper on thin film PV systems.[1] The optoelectronic properties for SnS such as

free carrier concentration and density of states were used from B. Subramanian et. al's paper, [5] while the absorption profile was calculated from the work of Brownson et. al.[6]

5.2. Results and discussion

It is observed in Figure 4.2 that the voltages have opposite polarities for the two device schemes. This is due to the fact that AMPS calculates all potentials relative to the reference vacuum level at the right end of the device (i.e. at the rear contact), and that the two devices have current flows in opposite directions which is responsible for this difference. To ease comparing simulations, the negative currents have been moved from quadrant III to quadrant II. Figure 4.2 represents a superimposed image of the two plots along the positive current axis.

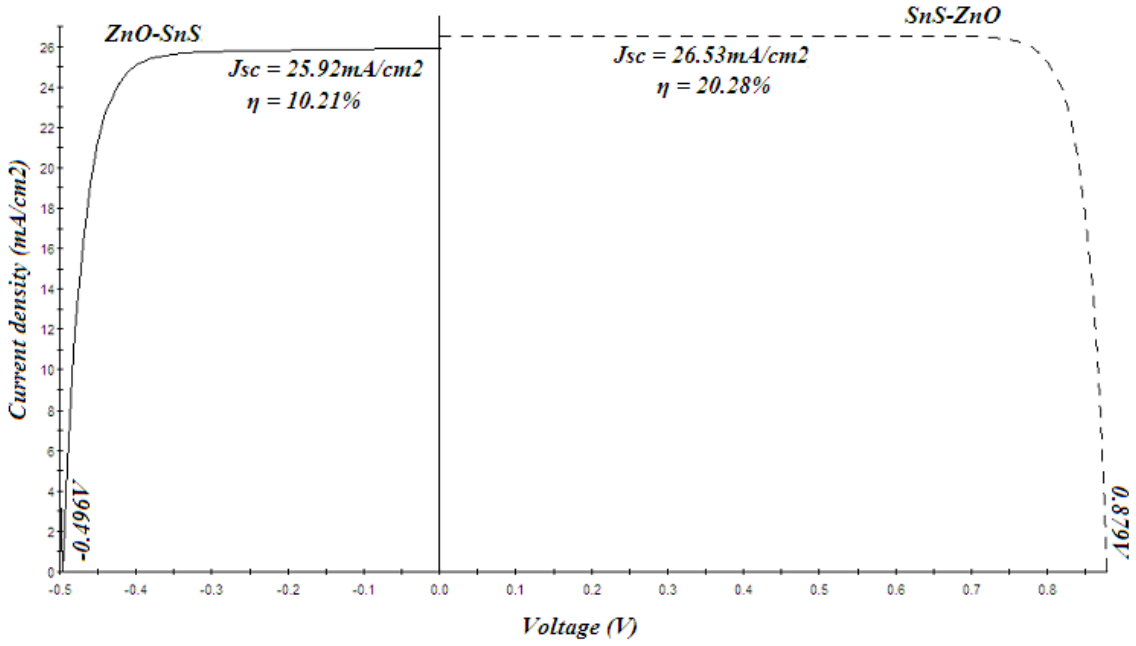

Figure 5.2: Simulated J-V characteristics of the *oxide-absorber* (solid) and *absorber-oxide* (dashed) PV devices under illumination.

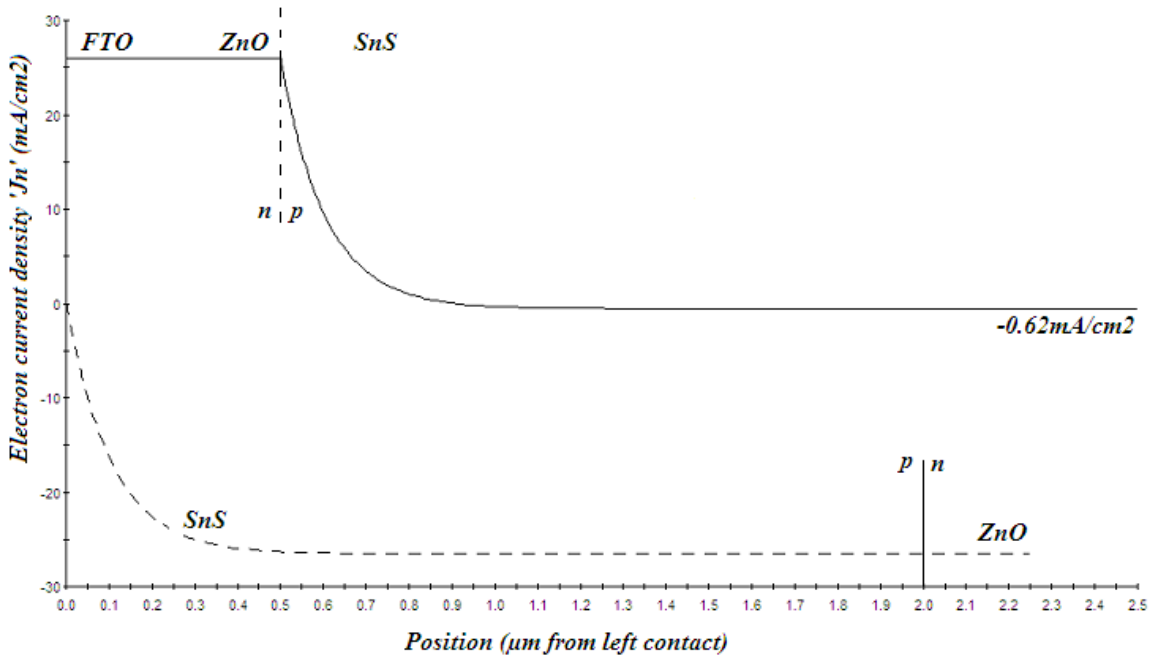

Figure 5.3: Spatial variation of minority carrier (electron) current densities in the absorber for the *oxide-absorber* (solid) and *absorber-oxide* (dashed) devices. The vertical lines indicate the positions of the respective electrochemical junctions.

We see in Figure 5.2 that current densities achieved in the *oxide-absorber* device are 26% lower than the theoretical limit (35 mA/cm^2 [7]) for absorbers of band gap 1.25 eV, suggesting good light absorption and photoconversion. This is further evident in Figure 5.3 where we observe no current losses in the window oxide (similar to what is observed in *sulfide*-based devices in Chapter 4) and the overall current is entirely attributable to the minority carriers at the front end of the absorber (x=0.5 µm). Note, however, that beyond 0.35µm into the SnS the minority currents become negative (0.62mA/cm^2) that suggest power losses in proportion to this value. This phenomenon is caused by the presence of unfavorable band energy equilibrium at the SnS|Cu interface at the rear end that actually promotes minority carrier injection into the metal. This feature can be seen in the region between 2.3-2.5µm in Figure 5.4 where electric fields in the space charge region of the absorber cause some photogenerated electrons to be injected into the copper and lost as heat.

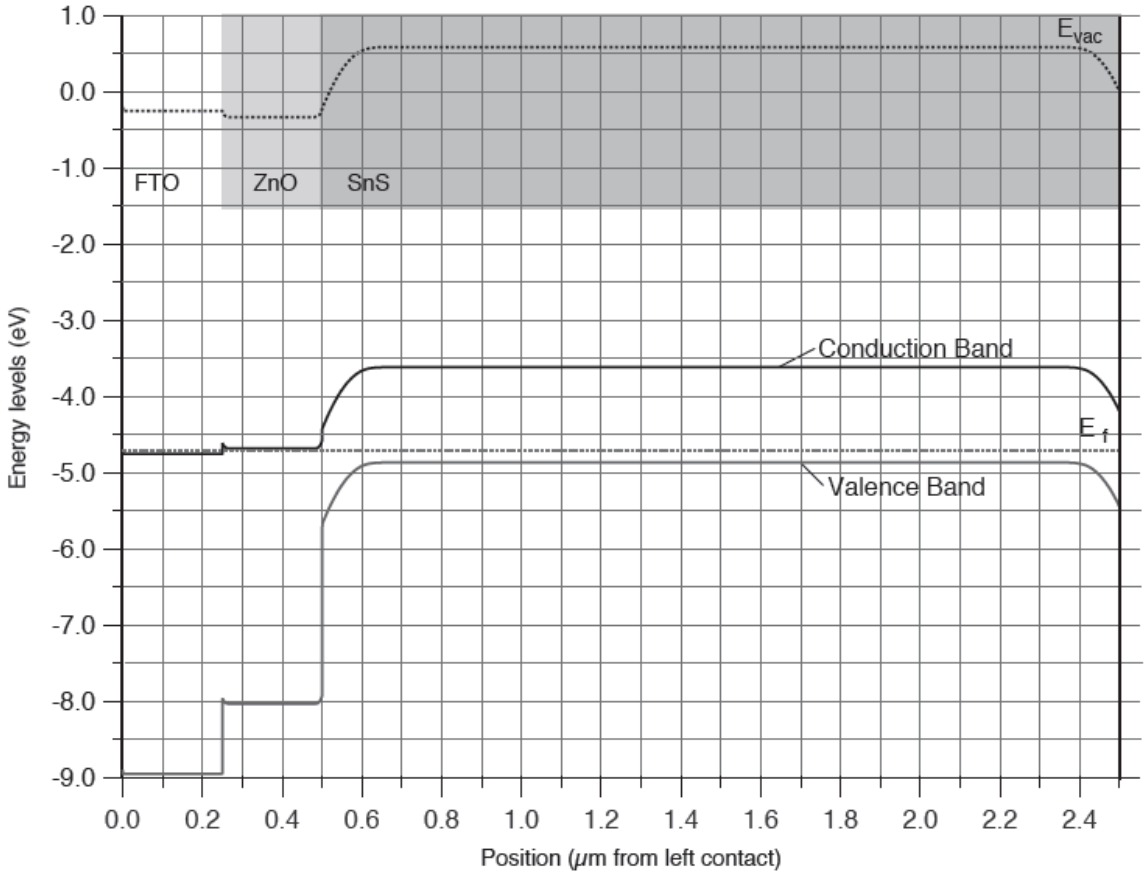

Figure 5.4: Energy band diagram of the *oxide-absorber* device under thermodynamic equilibrium (no illumination).

The high free electron concentrations (10^{20} cm^{-3}) in the TCO also cause the fermi level to be relatively pinned by this layer. This results in most of the space-charge region across the n-p interface to be accommodated in the absorber between 0.5-0.65 μm in Figure 5.4. The presence of strong electrostatic fields in this region should be responsible for the high collection of the photogenerated minority carriers by the window oxide layer that explains the current densities observed in these devices.

However, an inspection of Figure 5.2 reveals that the major cause of low efficiencies in *oxide-absorber* devices is the high voltage deficit (0.754 V). This is because of narrowing of the fermi level

splitting inside the absorber near the rear contact. As photogenerated electron-hole pairs are produced close to this region, the unfavorable band equilibrium causes electron quasi-fermi level to sharply decrease and approach that of the adjoining metal and, at the same time, causing the hole quasi-fermi level to increase 0.04 eV. This tailing down of electron quasi-fermi level to that of the copper is what causes minority carrier injection into the metal, and thus explains the negative current densities observed in this region in Figure 5.3. It must also be pointed out that the optical generation rates are about 7 orders lower in the rear depletion region compared to the front end of the absorber, and suggests that such unfavorable band alignments have a drastic influence on the fermi level splitting close to that region since a greater fraction of the photogenerated minority carriers are now injected into the metal and resulting in both current and voltage losses. It is therefore interesting to reverse the order of HJ formation with respect to the irradiance, and evaluate how the PV performance would be affected in such devices. As explained earlier, such devices also permit the use of platinum as ohmic contact material to SnS, and thereby promise higher conversion efficiencies.

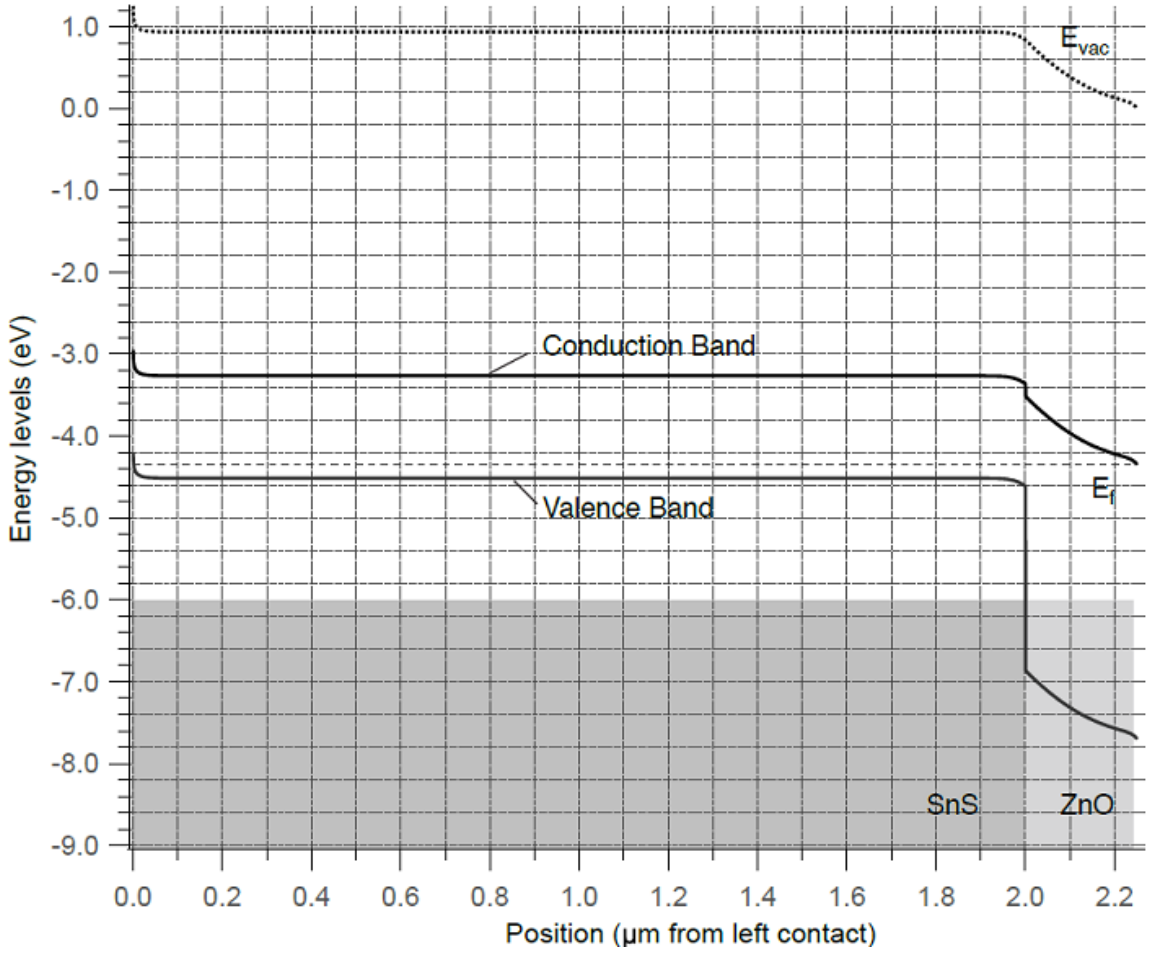

Figure 5.5: Energy band diagram of the *absorber-oxide* device under thermodynamic equilibrium (no illumination).

An inspection of Figure 5.2 indeed reveals superior PV performance in *absorber-oxide* devices, mainly attributable to enhanced open-circuit voltages. Also note in Figure 5.3 that there is no minority carrier current across the front end (at $x=0^{-}$) of such devices, which suggests no electron injection into the platinum. An inspection of the current densities of the two systems also reveals that their difference is entirely attributed to the negative current flows in the *oxide-absorber* devices. The absence of an FTO layer in Figure 5.5 is responsible for depletion regions in the absorber (between 1.95-2 µm) that are one-third in thickness compared to that in the other configuration, as significant band bending here occurs inside the oxide. However, in Figure 5.5 the presence of favorable band

alignments for hole transport at the front contact ensures the fermi level splitting is wide enough in the depletion region of the absorber ($0<x<0.05\mu m$) to generate the open-circuit voltages observed in Figure 5.2 for such devices. It is therefore evident that the platinum ohmic contact in the *absorber-oxide* cell is more critical to the high voltage predicted in such a design, and the weaker electric fields for minority charge injection into the n-type oxide have relatively less impact on the overall current densities observed in the two device schemes.

5.3 Summary

The favorable optoelectronic properties of SnS and its lower commodity and processing costs due to the greater availability and lower prices of the commodity elements tin and sulfur make the tin-based absorber material a more promising candidate for cost-effective photovoltaics in relation to the market incumbent CdTe. A comparative modeling of PV cells based on the ideal HJ between SnS and ZnO for two configurations relative to the irradiance suggests efficiency limitations in the *oxide-absorber* device (10.2%) due to the use of rear copper contact in lieu of the superior platinum metal (employed in the *absorber-oxide* device) that causes reverse electron current into the metal due to undesirable band energy equilibrium. Such unfavorable alignments in combination with lower optical generation rates at the absorber-metal contact cause the fermi level splitting between electrons and holes to narrow down at the interface, which critically reduces the open-circuit voltages achievable in such systems. On the other hand, the use of platinum supports higher voltages due to favorable band alignments and is also responsible for the absence of the negative current observed in the *oxide-absorber*. However, the current densities predicted for the two systems are very similar and suggest the relative insignificance of weaker electrostatic fields in the space charge region of the absorber at the p-n HJ on the overall current transport characteristics of the two device configurations. It should be expected that future research endeavors in SnS are based on the *absorber-oxide* design and could be the key to thin film PV cracking the 20% efficiency barrier at processing costs lower than CdTe or CIGS.

References

[1] M Gloeckler, AL Fahrenbruch, JR Sites. "*Numerical Modeling of CIGS and CdTe Solar Cells: Setting the Baseline*". 3rd conf. PV ener. conv.; 491-494; **2003**.

[2] B Ghosh, M Das, P Banerjee, S Das. "*Fabrication of the SnS/ZnO Heterojunction for PV Applications Using Electrodeposited ZnO Films*". Semicond. Sci. Technol. 24; 025024 (1-7); **2009**.

[3] USGS http://minerals.usgs.gov/minerals/pubs/commodity/platinum/mcs-2011-plati.pdf (Accessed Dec. 10th **2011**)

[4] First Solar Corporate Overview Q3 2011.

http://files.shareholder.com/downloads/FSLR/1522835684x0x477649/205c17cb-c816-4045-949f-700e7c1a109f/FSLR_CorpOverview.pdf (Accessed Dec. 10th **2011**).

[5] **B Subramanian, C Sanjeeviraja, M Jayachandran "*Cathodic Electrodeposition and Analysis of SnS Films for Photoelectrochemical Cells*". Mat. Chem. & Phys. 71; 40–46; 2001.**

[6] JRS Brownson, C Georges, CL-Clément. "*Synthesis of a δ-SnS Polymorph by Electrodeposition*". Chem. Mater. 18; 6397-6402; 2006.

[7] SJ Fonash. Solar Cell Device Physics. 2nd edition Elsevier, USA; 2010.

Chapter 6

Identifying photovoltaic efficiency limits in CZTS-based devices

In this Chapter, CZTS has been numerically evaluated for PV conversion efficiencies and compared with the results for binary SnS presented in the previous Chapter. This study evaluates baseline cells based on the ZnO|CdS|CZTS heterostructure (herein referred to as *oxide-sulfide-absorber* device) for two different TCO materials (FTO and ITO) using AMPS-1D and quantifies reasons for the efficiency limits predicted in such devices. The performance of CZTS cells upon reversal of the order of stacking layers (with respect to light incidence) is also evaluated for the CZTS|CdS|ZnO structures (referred to in this chapter as *absorber-sulfide-oxide* devices) and compared to those developed using the binary SnS as the light absorbing constituent. An approach to high efficiency PV based on the tin-absorber system is presented based on the results from this study.

6.1 Materials selection and methodology

It has been demonstrated in the previous Chapter that cells based on the FTO|ZnO|SnS system reveal superior current densities compared to the ITO|CdS|SnS devices. However, the most efficient cells developed yet with CZTS employ the ITO|ZnO|CdS|CZTS configuration and a comparison in conversion efficiencies is needed for the ZnO|CdS|CZTS cells that employ ITO and FTO as the TCO layer.[1] The most efficient lab cells based on this system have been modeled in this study and have the configuration represented on the right of Figure 6.1.[1] The only variation from the practical cells is that this study employs platinum as the ohmic contact to the absorber instead of the molybdenum typically employed. This deviation is done assuming ideal contact between the metal and CZTS based on theoretical work function values. As explained in the earlier Chapter, the use of platinum in such a role would be cost-prohibitive; however the aim in this study is to evaluate the maximum theoretical efficiencies attainable with CZTS-based PV devices and identify scope for enhancements based on these values.

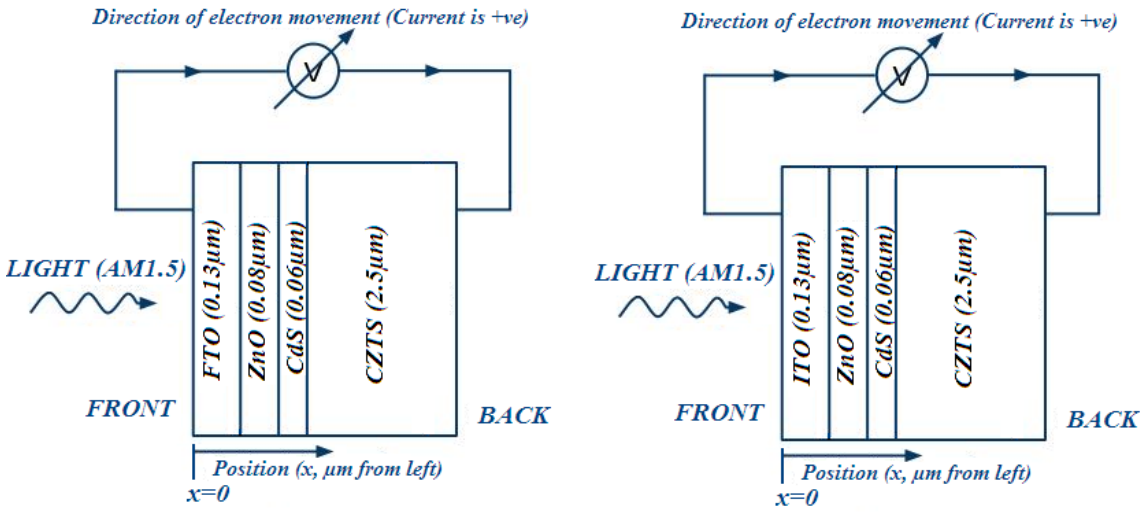

Figure 6.1: Schematic of the two ZnO|CdS|CZTS based PV devices employing FTO (left) and ITO (right) as the TCO layers. The different material layers are not drawn to scale. The platinum contact to the absorber is not part of the main device structure and hence is not represented here (it lies right of the CZTS layer). Please refer to Appendix A for conventions.

The optoelectronic properties of the different material layers used in this study have been taken from Gloeckler's baseline paper on thin film PV systems [2]. The different material properties of CZTS such as free carrier concentration, energy gaps, and density of states were used from N. Amin et. al's paper [3], while the absorption profile was calculated from the work of Riha et. al. [4].

6.2 Results and discussion

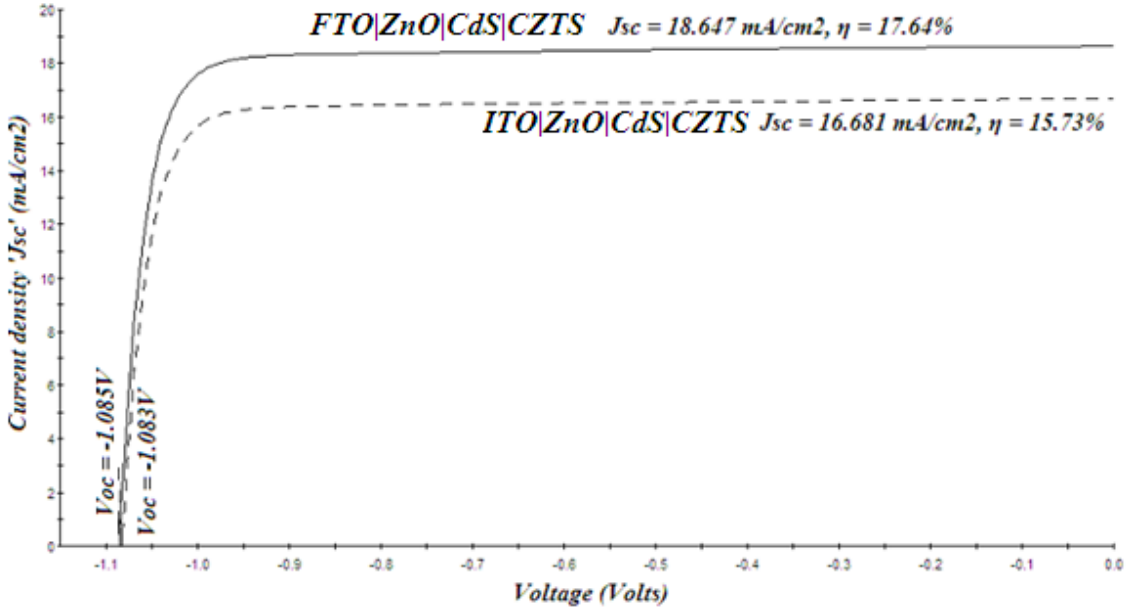

Figure 6.2: Illuminated J-V characteristics of the *oxide-sulfide-absorber* cells based on ITO (dashed) and FTO (solid) as the TCO.

Figure 6.2 compares the calculated current densities (J) as a function of voltage (V) for the two device schemes. It should be noted that the open-circuit potentials generated are almost identical, which is expected given the similarity in the respective back ohmic contacts that most critically influence voltages. However, the difference in efficiencies of 1.9% is due to variations in short-circuit current densities caused by the changing electron transport properties at the TCO|ZnO interface.

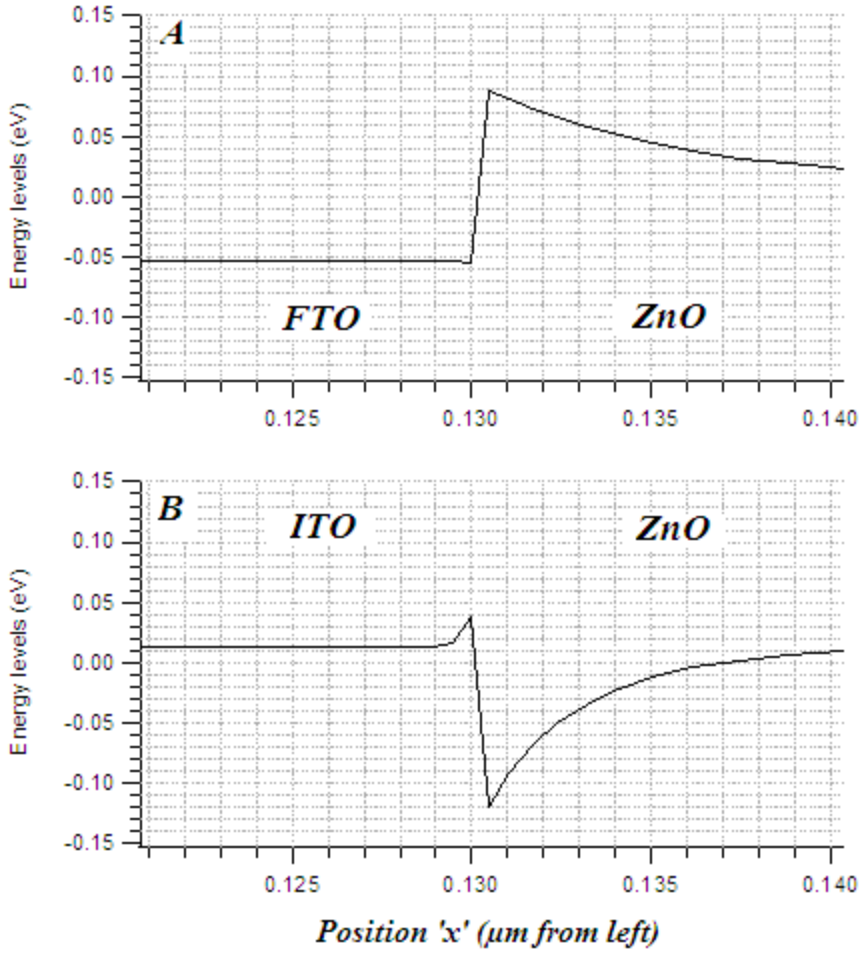

Figure 6.3: Variations in conduction band energy levels at (A) the FTO|ZnO and (B) ITO|ZnO interfaces for the illuminated *oxide-sulfide-absorber* devices at short-circuit. The electrochemical junction is at x = 0.130µm.

For the ITO|ZnO device, Figure 6.3(B) indicates that the electrons in ZnO that reach the HJ interface at x=0.130µm from the neighboring CdS layer accumulate at the junction. The accumulation of electrons is due to the effective potential of 0.16 V encountered there under short-circuit conditions due to the differing conduction and fermi energy levels between the TCO and the ZnO. However, in the case of FTO|ZnO (Figure 6.3(A)), the band offset of 0.14 eV is favorable for electrons to be collected by the front TCO layer. Since electrons are majority carriers in these layers, they will be able to overcome the electric field barrier at the space charge region of ZnO (between 0.13-0.14µm in Figure 6.3(A)) and contribute to

current flow. It could be argued that the pile-up phenomenon in ITO|ZnO devices would instead result in a drop in the open-circuit voltage relative to the FTO|ZnO cell. This is explained in terms of the transport theory equation based on which carrier currents are computed [5]. Note that electron current densities are given by:

$$J_n = q \cdot \mu \cdot n \cdot {dE_{fn}}/{dx} \qquad \text{Eq. (6.1)}$$

where Ef_n is the quasi-fermi level of electrons upon illumination, μ is the electron mobility, n is the free electron concentration, and q is the electronic charge. Note that the majority carrier concentrations do not vary drastically upon illumination i.e. 'n' is relatively unchanged. This implies that from eq. (6.1) any small change in their quasi-fermi levels should cause significant variations in the value of J_n. Consequently, when the accumulated electrons at the interface recombine at the end of their lifetimes, there is a slight change in their quasi-fermi level at the electrochemical junction that is significant enough to cause the current density values to reduce relatively, seen in Figure 6.2.

The band features observed in Figure 6.3 are due to the higher free carrier concentrations in FTO ($3.5x10^{20}$ cm^{-3}) compared to ITO (10^{20} cm^{-3}) and a higher electron affinity in the former material compared to the latter that produces better band alignments with the ZnO. The efficiencies predicted here for FTO-*oxide-sulfide-absorber* devices are higher than the values for the corresponding *oxide-absorber* devices (η=10.2%) described in Chapter 4, but still lower than the 20% value demonstrated to be achievable in the *absorber-oxide* device configurations (reproduced from Chapter 5 in Figure 6.4). It should hence be relevant to probe the FTO-based CZTS device under inverted configuration (the *absorber-sulfide-oxide*) with respect to light incidence and identify efficiency limits relative to the SnS-based system.

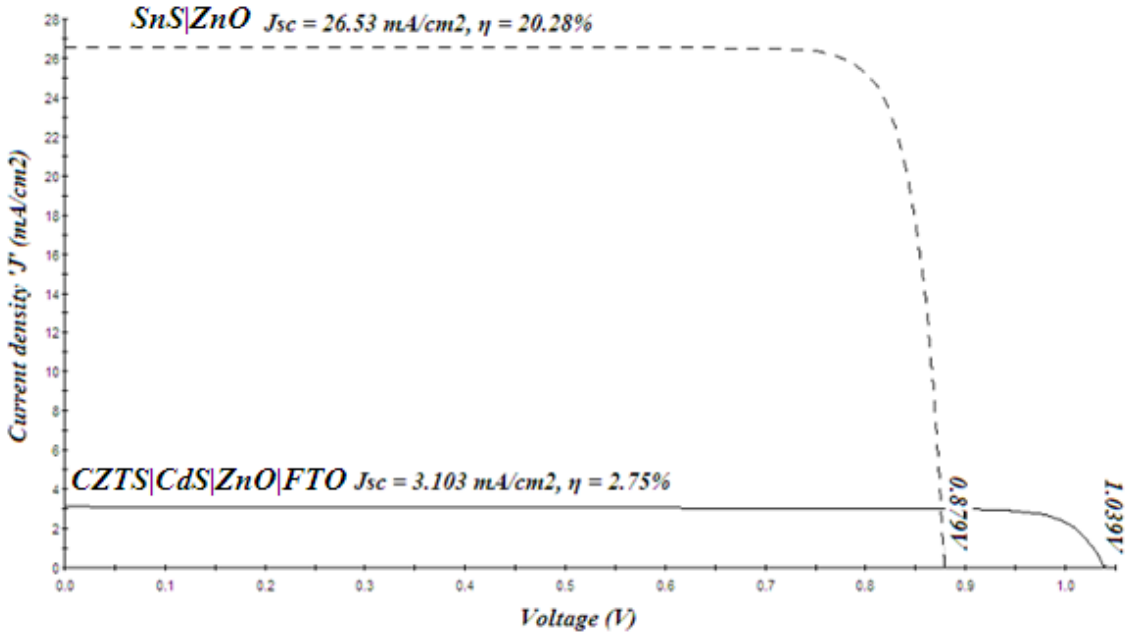

Figure 6.4: Illuminated J-V plot of the *absorber-sulfide-oxide*-FTO device (solid), corresponds to the reverse illumination of the device in Figure 6.1. The J-V characteristic of the SnS|ZnO cell (dashed) is also given here for reference.

It is interesting to note in Figure 6.4 that direct absorption of irradiance by the quaternary absorber causes drastic reduction in the predicted efficiencies of *absorber-sulfide-oxide*-FTO systems from 17.64% (cf. Figure 6.2) to 3.1%. Further inspection reveals decrease in short-circuit current densities as the chief contributing factor for efficiency lowering whereas the open-circuit voltages are relatively unchanged.

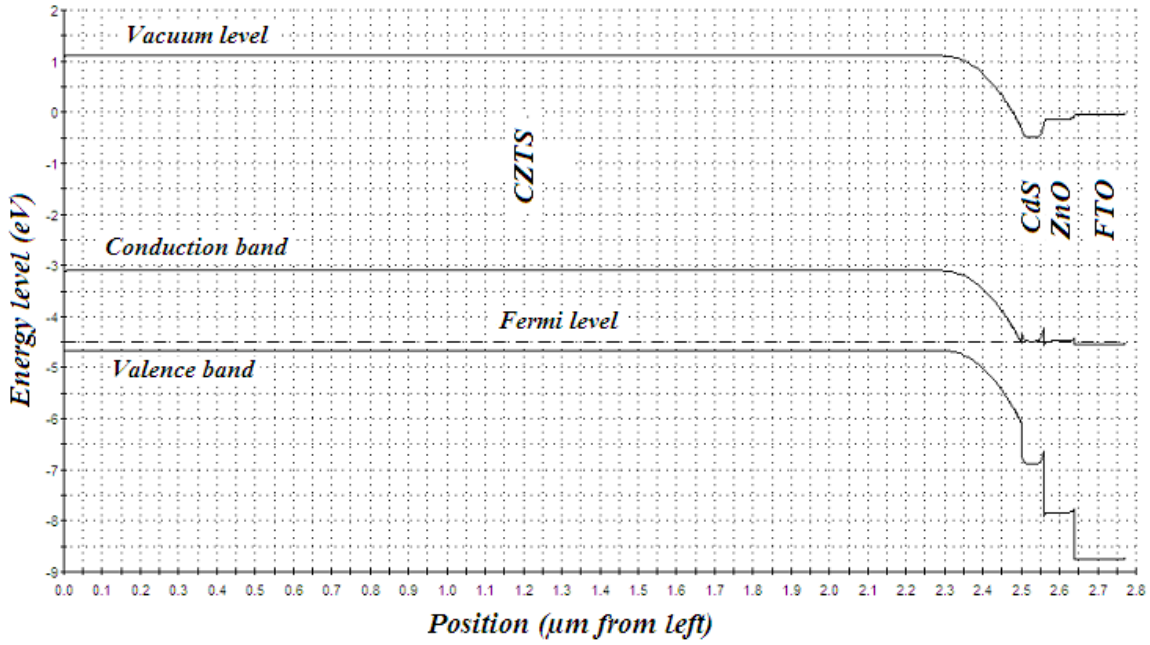

Figure 6.5: Energy band diagram of the *absorber-sulfide-oxide*-FTO PV device under thermodynamic equilibrium (TE).

To explain the cause of low current densities in the front illuminated CZTS PV device, an inspection of Figure 6.5 indicates the absence of a space-charge region near the front surface of the absorber (x=0) that can provide a favorable electric field for photogenerated electron-hole separation and conduction through the overlying platinum contact. It should be noted that absorption (and consequently, carrier photogeneration) is the highest at the front end and hence, diffusive movement of minority carriers should dominate close to this region of the absorber, while drift-based injection into the CdS starts dominating transport closer to the rear p-n HJ interface (x=2.5 μm). Figure 6.6 indicates strong electron and hole currents near the front end that are both occurring in the same direction, as evident from their opposing signs. Per AMPS convention, this implies both holes and electrons are flowing toward the front end, which opposes the drift-diffusion mechanism just explained. Hole movement in this direction is attributed to the drift component of the effective force developed because of the presence of the Schottky barrier at the rear interface. The absence of a space-charge region in the front end of the absorber that can similarly

act as a Schottky barrier to electron movement causes electrons to be injected into the front platinum, and results in great reductions in current densities through surface recombination. This phenomenon at contacts typically has a large value 10^7 cm/s and is incorporated in the model to account for the presence of a high concentration of dangling bonds, impurities, and other adsorbed species that can serve as recombination centers and contribute to the lowering of current densities. It is therefore concluded that the direct absorption configuration of the irradiance generates high conversion efficiencies only if the front ohmic contact provides a sufficiently positive electrostatic field for majority carrier transfer across the interface, and that the absence of such a region can be deleterious to device performance. In fact, this is the reason for the top PV efficiencies observed in the *absorber-oxide* models (cf. Figure 6.4) that provide an avenue for future device development based on the tin-absorber system.

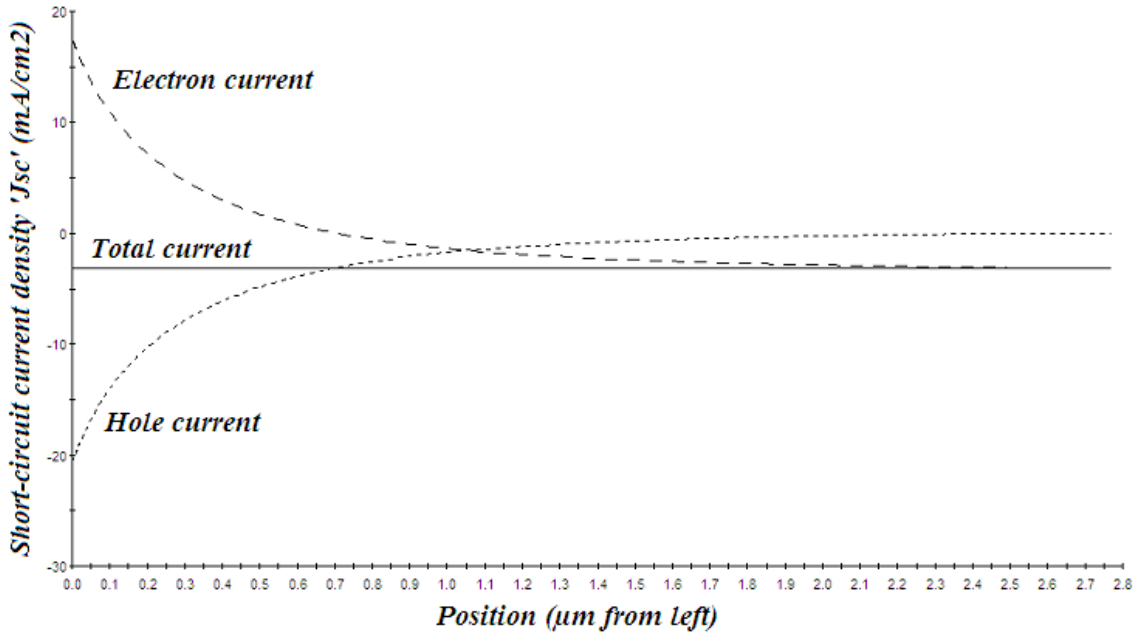

Figure 6.6: Spatial variation in electron (dashed) and hole (dotted) short-circuit current densities for the *absorber-sulfide-oxide*-FTO device under illumination.

6.3 Remarks and summary

Baseline PV devices based on the CZTS absorber system and utilizing either FTO or ITO as the TCO layer have been numerically evaluated for their conversion efficiencies and the differences explained in terms of the underlying charge transport phenomena. Ideal ohmic contacts based on platinum have been assumed in this work and no economic constraints have been imposed on the use of this metal as the rear contact so that the maximum theoretical efficiencies attainable with such devices may be evaluated. Since no PV cell in this configuration promised greater than 20% efficiency, the back-illumination approach that was highly successful in SnS PV was considered. However, this configuration greatly decreases efficiencies in CZTS cells due to unfavorable band alignments at the platinum-absorber contact that promotes surface recombination by serving as a sink for photogenerated electrons from the underlying semiconductor layer.

The absence of the space-charge region at the front metal-CZTS interface, unlike in the case of SnS-based PV devices, is a consequence of the high hole affinities observed in this compound (5.77 eV) compared to the binary sulfide (5.45 eV). Though their electron affinities are almost identical, the wider band gap of CZTS (1.56 eV) compared to SnS (1.25 eV) makes PV conversion based on such devices sub-optimal, and suggests band gap reductions through substitutional alloying and lattice modification of the parent kesterite. This is consistent with the fact that the highest lab efficiencies of CZTS cells have a band gap of 1.2eV,[1] instead of the more optimal 1.4-1.5 eV. Such reductions have been achieved by substituting the sulfur anion sublattice with selenium atoms so that the conduction band levels may be lowered. However, increasing efficiencies up to 20% require lower band gaps arising from smaller hole affinities, which indicates the need for cationic substitution instead. The binary SnS can be lattice modified with copper and/or zinc substitution to yield semiconductor materials with optimal absorption properties for PV conversion. It has also been thermodynamically established that the Cu-Sn sublattice tends to form charge-compensated defect complexes [Cu_{Sn} + Sn_{Cu}] that passivate the relatively deep levels in the kesterites, and thereby benefit absorber performance.[6,7] The band gap-modified SnS absorber under the

absorber-oxide configuration could present the best material for high efficiency PV devices required over the next several years.

References

[1] TK Todorov, KB Reuter, DB Mitzi. "*High-Efficiency Solar Cell with Earth-Abundant Liquid-Processed Absorber*". Adv. Mater. 22; E156-E159; **2010**.

[2] M Gloeckler, AL Fahrenbruch, JR Sites. "*Numerical Modeling of CIGS and CdTe Solar Cells: Setting the Baseline*". 3rd Conf. PV ener. Conv.; 491-494; **2003**.

[3] N Amin, MI Hossain, P Chelvanathan, ASMM Uzzaman, K Sopian. "*Prospects of Cu_2ZnSnS_4 (CZTS) Solar Cells from Numerical Analysis*". 6th Int. Conf. Elec. Comp.Engg.; 730-733; **2010**.

[4] SC Riha, SJ Fredrick, JB Sambur, Y Liu, AL Prieto, BA Parkinson. "Photoelectrochemical Characterization of Nanocrystalline Thin-Film Cu_2ZnSnS_4 Photocathodes". Appl. Mat. Interf.; 3(1); 58-66; **2011**.

[5] J Arch, J Hou, W Howland, P McElheny, A Moquin, M Rogosky, F Rubinelli, T Tran, H Zhu, SJ Fonash. "*A Manual for AMPS 1-D BETA Version 1.00*". **1997**.

[6] S Chen, J-H Yang, XG Gong, A Walsh, S-H Wei. "*Intrinsic point defects and complexes in the quaternary kesterite semiconductor Cu_2ZnSnS_4*". Phys. Rev. B 81; 245204 (1-10); **2010**.

[7] I Repins, N Vora, C Beall, S-H Wei, Y Yan, M Romero, G Teeter, H Du, B To, M Young, M Noufi. "*Kesterites and Chalcopyrites: A Comparison of Close Cousins*". NREL Preprint, Presented at the Mat. Res. Soc. Spring Meeting **2011.**

Chapter 7

Conclusions

In this dissertation, tin monosulfide (SnS) has been evaluated for performance as a light absorbing material for thin film photovoltaic structures. Numerical models developed using Analysis of Microelectronic and Photonic Structures (AMPS-1D) reveal efficiencies of cells under AM1.5 illumination based on three ideal n-p heterojunctions: CdS|CdTe, CdS|SnS and ZnO|SnS and identify avenues for further efficiency improvements in SnS PV device design based on increases in short-circuit current densities or open-circuit voltages. Similar external photoconversion efficiencies (10.1-10.2%) are predicted for the ITO|CdS|CdTe and FTO|ZnO|SnS device models, with the higher voltages in CdTe compensated by greater current densities observed in the latter. ITO|CdS|SnS device models display slightly lower efficiency due to absorption losses but offer lower voltage deficit compared to CdTe structures. The lower voltage deficit reveals ohmic contact behavior between copper and absorber in the FTO|ZnO|SnS structure compared to the ITO|CdS|CdTe device. Since this contact is the most critical part of the device that influences open-circuit voltage values, it should be interesting to invert the heterojunction between ZnO and SnS with respect to the irradiance and probe the device to identify efficiency limits. It could also be possible to increase the optical band gap of the chalcogenide closer to the ideal value (1.5 eV) by lattice dissolution and modification into CZTS. The wider band gap of CZTS should yield greater open-circuit voltages and has been increasingly researched as a PV material in the past few years.

A comparative modeling of PV cells based on the ideal junction between SnS (*absorber*) and ZnO (*oxide*) for two configurations relative to the irradiance suggests efficiency limitations in the *oxide-absorber* device (η=10.2%) due to the use of back copper contact in lieu of the superior platinum (employed in the *absorber-oxide* device). The *absorber-oxide* configuration is not considered in case

of CdTe because of the practical requirement to etch the absorber surface to produce a heavily doped metal telluride layer that can support photogenerated majority charge carrier transport. In the *oxide-absorber* configuration, the use of copper due to economic constraints causes reverse electron current into the metal due to undesirable band energy equilibrium that results in surface recombination. Such unfavorable alignments in combination with lower optical generation rates at the absorber-metal contact cause the fermi level splitting between electrons and holes to narrow down at the interface, which critically reduces the open-circuit voltages achievable in the *oxide-absorber* systems. On the other hand, the use of platinum supports higher voltages due to favorable band alignments in the *absorber-oxide* device (η = 20.2%) and is also responsible for the absence of the negative current observed in the *oxide-absorber*. However, the current densities predicted for the two systems are very similar and suggest the relative insignificance of weaker electrostatic fields in the space charge region of the absorber near the electrochemical junction (with *oxide*) on the overall current transport characteristics of the two device configurations. The higher open-circuit voltages and efficiencies predicted in the *absorber-oxide* configuration indicate that this design should be the approach for developing SnS into a high-efficiency PV device.

The other approach to increasing voltages is based on the CZTS absorber system as such cells have already demonstrated laboratory efficiencies of 9.6%.[3] Baseline cells utilizing either FTO (F-doped SnO_2) or ITO (Indium tin oxide) as the TCO (transparent conductive oxide) layer have been numerically evaluated for their conversion efficiencies and the differences explained in terms of the underlying charge transport phenomena. Ideal ohmic contacts based on platinum have been assumed in this work and no economic constraints have been imposed on the use of this metal as the rear contact so that the maximum theoretical efficiencies attainable with such devices may be evaluated. The calculated efficiencies show values lower than that for the *absorber-oxide* configuration, revealing that this design approach may be pursued (i.e. order of layer stacks inverted with respect to irradiance) with CZTS as well. However, modeling of this configuration revealed vastly lower

efficiencies in CZTS cells due to unfavorable band alignments at the platinum-absorber contact. The unfavorable alignments promote surface recombination by serving as a sink for photogenerated electrons from the underlying semiconductor layer.

The absence of the space-charge region at the front metal-CZTS interface, unlike in the case of SnS-based PV devices, is a consequence of the high hole affinities observed in this compound (5.77eV, relative to the local vacuum level) compared to the binary sulfide (5.45eV). Though their electron affinities are almost identical, the wider band gap of CZTS (E_g = 1.56eV) compared to SnS (E_g = 1.25eV) makes PV conversion based on such devices sub-optimal, and suggests band gap reductions through substitutional alloying and lattice modification of the parent kesterite. This is consistent with the fact that the highest lab efficiencies of CZTS cells have a band gap of 1.2 eV, instead of the more optimal 1.4-1.5 eV. Such reductions have been achieved by substituting the sulfur anion sublattice with selenium atoms so that the conduction band levels may be lowered. However, increasing efficiencies up to 20% would require lower band gaps arising from smaller hole affinities and suggests the need for cationic substitution instead.

It is concluded that absorbers having a band gap intermediate between the binary SnS and the quaternary CZTS (i.e. in the range 1.2-1.3 eV) could provide the most optimal semiconductor materials for optoelectronic conversion. Such a light absorbing material may be synthesized through suitable cationic substitutions in the SnS crystal structure. Future research efforts should look to address the impact of copper and zinc substitution on the orthorhombic SnS in terms of band structure modifications and the thermodynamic formation energy levels of the different defect chemistries permitted in such alloy systems. It should be noted that the Cu-Sn sublattice in CZTS has a tendency to form charge-compensated defect complexes [Cu_{Sn} + Sn_{Cu}] that passivate the relatively deep levels in the kesterites and thereby benefit absorber performance through reduced recombination rates.[4,5] However, the difference in tin valence states between CZTS (+4) and SnS (+2) would indicate different defect chemistries in the two systems, and requires greater theoretical understanding. It is

concluded that devices utilizing lattice-modified tin-based absorbers and adopting the direct irradiance configuration could be the answer to thin film PV attaining efficiencies beyond 20%.

7.1 Major research thrusts for future tin-based PV

The goal of this dissertation was to identify suitable materials for PV device formation with tin absorber systems and model the different configurations to numerically quantify efficiency limits to the various systems and help narrow the choices of materials based on both optoelectronic properties and external factors such as economic constraints and raw material criticality that are an integral part of low cost PV manufacturing. Consequently, all junctions assumed in this research are considered to behave ideally, in the absence of experimental information on possible structural and chemical phenomena that can promote non-ideal charge transfer characteristics across junctions through interface states. However, experiences with CdTe development show that there is no real correlation between theoretical and measured barrier heights at absorber-metal contacts due to the presence of various dipole states at the interface.[6] Since the metal contact is integral to the voltages predicted from models, the next step would be to experimentally deposit metals such platinum on SnS and measure the barrier height difference. Actual experimental values will greatly improve the order of accuracy of AMPS models, which can in turn be used to identify optimal structures for high efficiency solar cells. The iterative process between experiments and models is represented in the relationship between stages B and C shown in Figure 6.1, and will be crucial to tin-based PV quickly maturing from its nascent phase into step E and beyond. Part of the evolution process can also include development of optimal synthesis processes for large scale depositions so that the newly developed cells are not restricted in stage E (as in CIGS) and can be commercialized into PV products at affordable prices (step G). It is expected that as more and more experimental data on the electrical and physical properties of tin materials become available the role of simulation tools such as AMPS would become more crucial in developing models that aid critical decision making and help hasten the growth of tin-based technology as the next generation source of PV electricity.

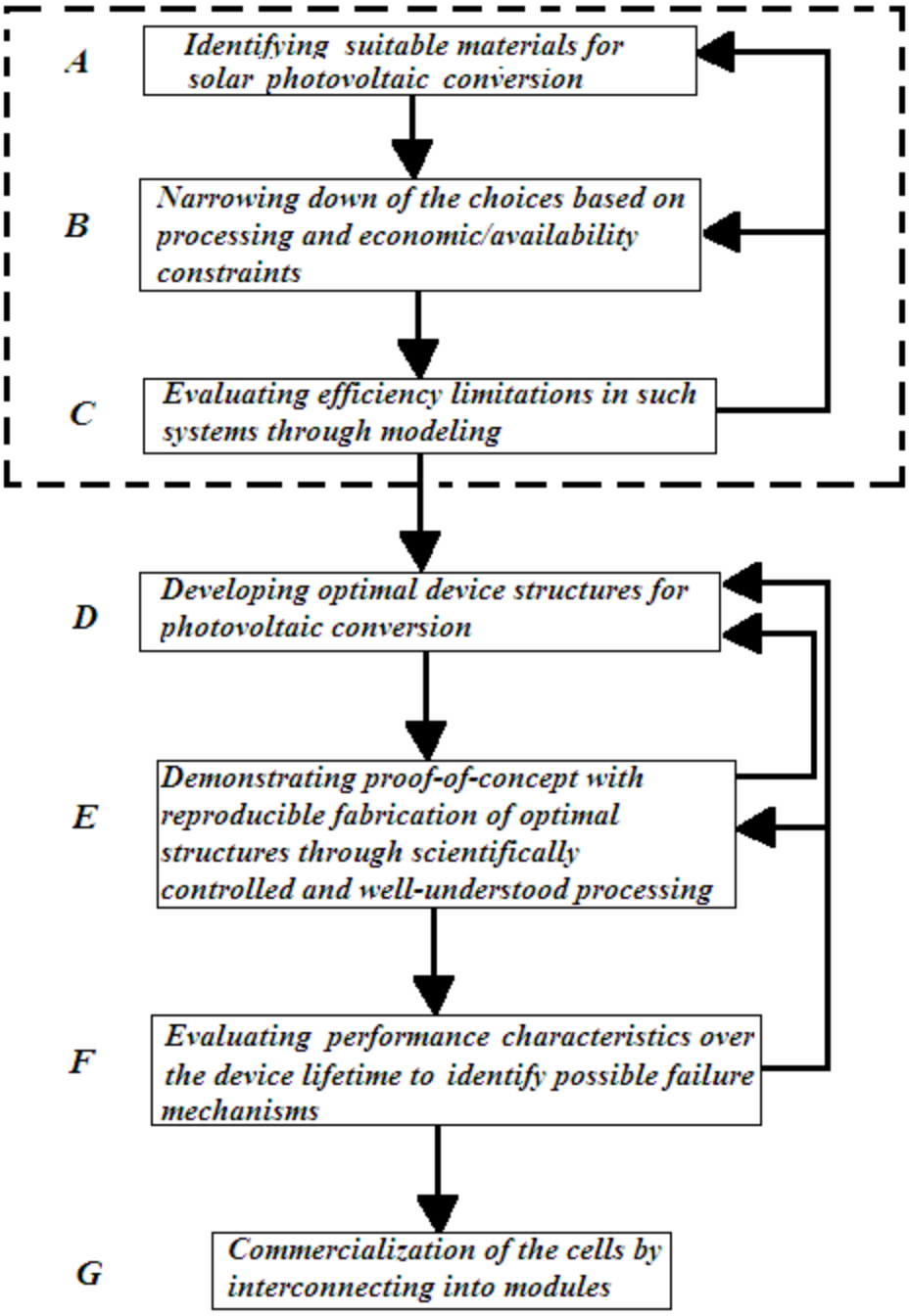

Figure 7.1: A flow chart illustrating the various stages in photovoltaic device development. The dotted rectangle represents the scope of this dissertation.

References

[1] CA Wolden, J Kurtin, JB Baxter, I Repins, SE Shaheen, JT Torvik, AA Rockett, VM Fthenakis, ES Aydil. "*Photovoltaic Manufacturing: Present status, future prospects, and research needs*". J. Vac. Sci. Technol. A 29 (3); 030801 (1-16); **2011**.

[2] W Shockley, HJ Queisser. "*Detailed Balance Limit of Efficiency of p-n Junction Solar Cells*". J. Appl. Phys. 32 (3); 510-519; **1961**.

[3] NREL: Best Research Cell Efficiencies. http://www.nrel.gov/ncpv/images/efficiency_chart.jpg (accessed Dec 9th 2011).

[4] S Chen, J-H Yang, XG Gong, A Walsh, and S-H. Wei. "*Intrinsic point defects and complexes in the quaternary kesterite semiconductor Cu_2ZnSnS_4*". Phys. Rev. B 81; 245204 (1-10); **2010**.

[5] I Repins, N Vora, C Beall, S-H Wei, Y Yan, M Romero, G Teeter, H Du, B To, M Young, M Noufi. "*Kesterites and Chalcopyrites: A Comparison of Close Cousins*". NREL Preprint, Presented at the Materials Research Society Spring Meeting 2011.

[6] AL Fahrenbruch. "Exploring Back Contact Technology to Increase CdS/CdTe Solar Cell Efficiency". Presented at the Materials Research Society Spring Meeting 2007.

Appendix A

Nomenclature and conventions used in this dissertation

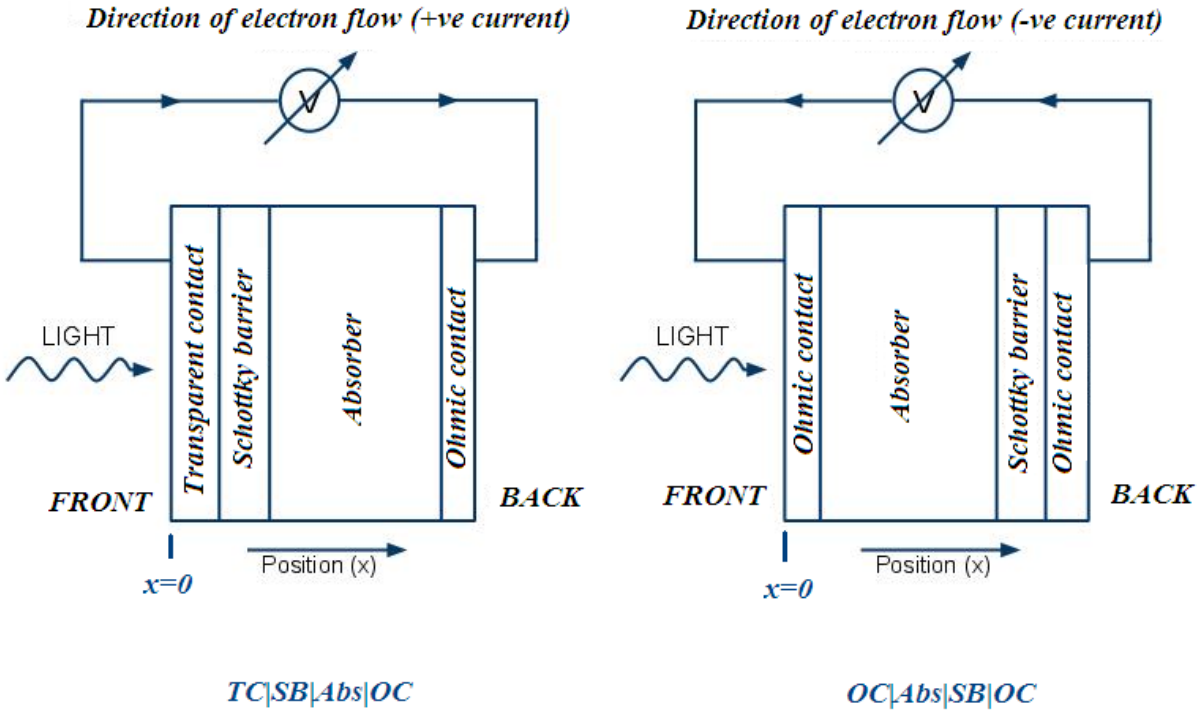

The figure shows two different configurations of solar cells with the different material layers. Note that the surface on which light is incident is always termed the "*front*" side or "*front*" end, while the surface through which light is transmitted is termed the "*back*" or "*rear*" end. In this work all light radiation is incident from the left, so the terms *front* and *left* may be used interchangeably (as are *back* and *right*).

The left configuration is represented by the notation shown below where TC refers to the transparent contact, SB refers to the Schottky barrier, Abs refers to the absorber, and OC is the ohmic contact. The notations are always written from left to right in the order in which light radiation passes through the device layers, and each vertical line represents an electrochemical junction between two different

materials. The position coordinate is measured from the left (or front) end and is positive to the right. The right configuration shows the reversal of device layers with respect to incident light.

Note that the function of the Schottky barrier material is to form an energetically unfavorable condition for the transport of majority carriers from the absorber so that these charges (typically holes, as most absorbers are p-type) can be driven to the ohmic contact meant for their collection. This contact is present to the right of the absorber in the left configuration, and to the left in the right configuration. It is also customary to refer to this layer when used in the left configuration as "window" material since it absorbs and transmits the incident radiation to the absorber. Note that electrons are collected at the left end in the left device and at the right end in the right configuration. Per convention used in models, this would correspond to positive and negative directions of currents.

The absorbers used in this dissertation are SnS, CdTe and CZTS (Cu-Sn-Zn-S). The Schottky barrier materials studied are CdS (referred to as *sulfide*) and ZnO (referred to as *oxide*). The ohmic contacts are typically metals and those used in the study include platinum, copper and silver. The transparent contact is usually referred to as the TCO (transparent conductive oxide) because the most common materials used for this purpose are indium tin oxide (ITO) and fluorine-doped tin oxide (FTO). These are also the two materials used in this research.

It must also be mentioned that this notation should not be confused with the order in which such materials may be actually deposited one on top of the other. The usual practice is to start depositions on a glass substrate. This substrate can either be to the left of the front transparent contact in the left configuration or to the right of the back ohmic contact in the right configuration, or even viceversa. Whatever maybe the sequence of deposition steps, the surface of the device layer (excluding metal contacts) that is receiving the irradiance first would always correspond to the front end (i.e. x=0) of the nomenclature adopted here.

Appendix B

Optoelectronic properties of the different material layers used in AMPS modeling

			Density of Energy States (cm^{-3})		(relative to vacuum)			A: Acceptors D: Donors	
Material	Band Gap (eV)	Conductivity type	(i) Conduction Band	(ii) Valence Band	Electron Affinity (eV)	Electron Mobility ($cm^2/V/s$)	Hole Mobility ($cm^2/V/s$)	Free carrier Concentration (cm^{-3})	Relative Permittivity
SnS	1.25	p	$1.0*10^{19}$	$4.13*10^{19}$	4.20	25	100	(A) $7.4*10^{16}$	12.5
ZnO	3.35	n	$2.2*10^{18}$	$1.8*10^{19}$	4.35	25	100	(D) $1.0*10^{18}$	9
FTO	4.20	n	$1.2*10^{20}$	$7.0*10^{20}$	4.50	20	100	(D) $3.5*10^{20}$	10
ITO	3.60	n	$2.0*10^{20}$	$1.8*10^{19}$	4.10	50	75	(D) $1.0*10^{20}$	2
CdTe	1.50	p	$8.0*10^{17}$	$1.8*10^{19}$	3.90	40	320	(A) $2.0*10^{14}$	9.4
CdS	2.40	n	$2.2*10^{18}$	$1.8*10^{19}$	4.00	25	100	(D) $1.1*10^{18}$	10
CZTS (kesterite)	1.56	p	$2.2*10^{18}$	$1.8*10^{19}$	4.21	100	20	(A) $4.0*10^{16}$	10

Appendix C

Absorption profile of the different material layers used in AMPS modeling

	p-SnS	n-CdS	ITO	n-ZnO	FTO	p-CZTS
λ (μm)	α(cm^{-1})	α(cm^{-1})	α(cm^{-1})	α(cm^{-1})	α(cm^{-1})	α(cm^{-1})
900	8.047E+04	7.000E+02	8.000E+02	1.633E+02	1.000E+03	4.042E+03
880	8.860E+04	7.000E+02	8.000E+02	2.000E+02	1.000E+03	4.670E+03
860	8.860E+04	7.000E+02	8.000E+02	2.633E+02	1.000E+03	4.880E+03
840	9.486E+04	7.000E+02	8.000E+02	3.000E+02	1.000E+03	5.729E+03
820	9.486E+04	7.000E+02	9.000E+02	3.000E+02	2.000E+03	6.590E+03
800	9.486E+04	7.500E+02	9.000E+02	3.250E+02	2.000E+03	7.901E+03
780	9.831E+04	7.500E+02	1.000E+03	4.052E+02	2.000E+03	9.691E+03
760	1.060E+05	8.000E+02	1.000E+03	5.052E+02	2.000E+03	1.247E+04
740	1.020E+05	8.000E+02	2.000E+03	8.052E+02	2.000E+03	1.537E+04
720	1.020E+05	8.000E+02	3.000E+03	9.052E+02	2.000E+03	1.840E+04
700	1.060E+05	8.000E+02	4.000E+03	1.475E+03	2.000E+03	2.267E+04
680	1.060E+05	8.000E+02	4.000E+03	1.050E+03	3.000E+03	2.378E+04
660	1.020E+05	9.000E+02	5.000E+03	1.050E+03	3.000E+03	2.548E+04
640	1.020E+05	9.000E+02	7.000E+03	1.050E+03	3.000E+03	2.782E+04
620	1.020E+05	9.000E+02	8.000E+03	1.050E+03	3.000E+03	2.902E+04
600	9.831E+04	1.000E+03	1.000E+04	1.050E+03	4.000E+03	2.994E+04
580	9.831E+04	1.200E+03	1.000E+04	1.100E+03	4.000E+03	3.373E+04
560	9.831E+04	1.500E+03	2.000E+04	1.250E+03	4.000E+03	3.538E+04
540	9.831E+04	2.000E+03	2.200E+04	1.500E+03	5.000E+03	3.950E+04
520	9.831E+04	2.000E+04	2.300E+04	1.500E+03	5.000E+03	4.543E+04
500	9.655E+04	5.000E+04	2.300E+04	1.500E+03	5.000E+03	5.194E+04
480	9.831E+04	8.000E+04	2.400E+04	1.750E+03	6.000E+03	6.513E+04
460	9.831E+04	9.000E+04	2.400E+04	5.000E+03	7.000E+03	8.159E+04
440	9.486E+04	1.000E+05	2.500E+04	8.220E+03	8.000E+03	1.156E+05
420	9.655E+04	1.100E+05	2.600E+04	2.000E+04	8.000E+03	1.497E+05
400	9.486E+04	1.100E+05	2.600E+04	5.500E+04	9.000E+03	1.959E+05
380	9.486E+04	1.200E+05	3.000E+04	1.000E+05	1.000E+04	1.664E+05

VITA

Ramprasad Chandrasekharan

PERSONAL: Male, Indian

EMAIL: ramprasad@psu.edu

EDUCATION

Ph.D. Energy and Mineral Engineering, The Pennsylvania State University, University Park, **May 2012**.

Numerical Modeling of Tin-Based Absorber Devices for Cost-Effective Solar Photovoltaics

Advisor: Jeffrey R.S. Brownson.

M.Eng. Engineering Science and Mechanics, The Pennsylvania State University, University Park, **December 2007**.

M.Tech. Metallurgical & Materials Engineering, Indian Institute of Technology Madras (IIT Madras), Chennai, India, **August 2005**.

B.Tech. Metallurgical & Materials Engineering, Indian Institute of Technology Madras (IIT Madras), Chennai, India, **August 2005**.